NASA Technical Memorandum 106112
ICOMP–93–10

A Transfer Matrix Approach to Vibration Localization in Mistuned Blade Assemblies

Gisli Ottarsson
The University of Michigan
Ann Arbor, Michigan

and

Christophe Pierre
Institute for Computational Mechanics in Propulsion
Lewis Research Center
Cleveland, Ohio

and The University of Michigan
Ann Arbor, Michigan

May 1993

NASA

A Transfer Matrix Approach to Vibration Localization in Mistuned Blade Assemblies.

Gísli Óttarsson*
Department of Mechanical Engineering and Applied Mechanics
The University of Michigan
Ann Arbor, Michigan 48109-2125

and

Christophe Pierre†

Institute for Computational Mechanics in Propulsion
Lewis Research Center
Cleveland, Ohio 44135

and The University of Michigan
Ann Arbor, Michigan 48109-2125

Abstract

A study of *mode localization* in *mistuned bladed disks* is performed using *transfer matrices*. The transfer matrix approach yields the free response of a *general*, mono-coupled, perfectly cyclic assembly in closed form. A *mistuned* structure is represented by *random* transfer matrices, and the expansion of these matrices in terms of the small mistuning parameter leads to the definition of a measure of *sensitivity* to mistuning. An approximation of the *localization factor*, the spatially averaged rate of exponential attenuation per blade-disk sector, is obtained through *perturbation techniques* in the limits of high and low sensitivity. The methodology is applied to a common model of a bladed disk and the results verified by *Monte Carlo simulations*. The easily calculated sensitivity measure may prove to be a valuable design tool due to its system-independent quantification of mistuning effects such as mode localization.

*Graduate Research Assistant.
†Associate Professor.

1. Introduction

A perfectly periodic structure consists of a chain of identical elements connected to one another in an identical manner. If the last element of the chain is connected to the first one, the structure is said to have cyclic symmetry. When analyzing the dynamics of *bladed-disk assemblies* one frequently postulates perfect cyclic symmetry. This is equivalent to assuming that the bladed disk is tuned, that is, that all blades are strictly identical and are identically mounted and uniformly spaced on a homogeneous, symmetrical disk.

All cyclic structures share the same set of modes of vibration, called *constant interblade phase angle* modes[1]. The vibration modes are so named, because in a normal mode motion all blades vibrate with the same amplitude and the difference in phase between the motion of adjacent blades is constant throughout the blade assembly. This assumption of perfect cyclic symmetry simplifies drastically the vibration analysis of bladed disks. Instead of analyzing the structure as a whole, the equations of motion may be uncoupled and the size of the problem reduced to that of a single blade or that of a blade-disk sector. However, designers are aware of inherent differences among rotor blades, due to material and manufacturing tolerances as well as in-service degradation, a phenomenon referred to as *rotor mistuning*. While it is widely accepted that mistuning causes a reduction in the risk of flutter instability [1,2], it has also been established that mistuning has a negative effect that could outweigh this benefit, by increasing forced response amplitudes: Thus mistuning may alter the results of a tuned analysis drastically[3,4,6][2].

One of the most important problems that plague turbomachinery rotors is the existence of rogue blades — lone blades that exhibit unexpected fatigue failure. Recently it has been suggested that rotor mistuning might be the cause of rogue blades, through a phenomenon called normal mode localization, whereby vibrations are confined to a few blades of the assembly [2-4,6-9].

The phenomenon of vibration localization may be expected to occur in any nearly periodic structure for which perfect periodicity is prevented by small irregularities. Localization, like damping, manifests itself as a spatial decay of the vibration amplitude along the structure, but for vastly different reasons. In the case of damping, energy is dissipated as vibrations are transmitted through the system, whereas in the case of localization, the energy is merely confined to a small geometric region within the structure. Localization occurs because waves propagating away from the energy source are reflected by the boundary between the slightly different subsystems making up the nearly periodic structure. The resulting confinement of energy may lead to much higher amplitudes locally than would be predicted if perfect periodicity were assumed, with possibly disastrous effects, for example in turbomachinery. The localization phenomenon has recently received wide attention in the literature and it has been shown to occur in various types of nearly periodic structures, namely blade assemblies [2-4,6-9], multi-span structures [10-14], and some large space structures [15].

The manner in which the substructures, or bays, which make up a (nearly) periodic structure are interconnected plays a major role in its dynamics and in the occurrence of mode localization. It is only through these connections that vibrational energy is passed between substructures. If neighboring bays are connected through several degrees of freedom the periodic structure is said to be a multi-coupled or a multi-wave structure. Conversely, if neighboring bays are only connected through a single degree of freedom, the system is mono-coupled and it carries a single pair of left- and right-traveling waves [16].

Each bay in a (nearly) periodic system is, in general, a multi degree-of-freedom substructure which may or may not be connected to ground. In the work of Mead [16], a bay with at least one immovable point within is called "positive-definite" (for example, a multi-span beam on simple supports), whereas a "semi-definite" bay has no such immovable points (for example, a taut string with masses at regular intervals). In the case of a turbine rotor, each bay in the chain is a model of one blade and of an appropriate sector of the disk to which the blade is attached. These blade-disk elements are "positive-definite," since they have fixed points in the form of either an unmodeled (rigid) part of the disk to which the elements are attached or their common

---

[1] In the periodic structure literature these modes are often referred to as extended, or global modes. We shall make use of the latter terminology here.

[2] The numerous studies of the effect of mistuning on the dynamics of blade assemblies are reviewed in a survey paper by Srinivasan [5].

axis of rotation. Coupling between blades is due to structural coupling through the disk and aerodynamic coupling through the fluid. Blades may also be connected through a shroud. Hence a blade assembly is, in general, a complex multi-coupled (nearly) cyclic structure.

The dynamics of a tuned, multi-coupled blade assembly are modeled by matrices that have a circulant structure and are generally fully populated. Recall that a matrix is circulant if every line is a permutation of the previous line by a shift to the right by one element [17]. If several degrees of freedom are considered for each blade, the system matrices become block-circulant. The coupling between blades is generally strongest between neighboring blades, and becomes weaker as the blades are further apart. This leads to block-circulant matrices that are dominated by blocks close to the diagonal (and corresponding blocks near the top right and bottom left corners). The well-developed theory of circulant matrices [17] provides a valuable tool for the analysis of tuned cyclic systems. However, when cyclicity-breaking mistuning is introduced, the circulant structure disappears and another means of solution is desired.

If the strength of coupling between two blades in an assembly decreases rapidly with decreasing proximity, a blade might be considered to influence only a few of its close neighbors, by ignoring the effect it has on the rest of the blades. To capitalize on this assumption, a transfer matrix approach can be introduced. For example, an assembly which features only coupling between adjacent blades can be modeled efficiently with transfer matrices of dimension twice the number of coupling coordinates [16]. Note that the number of degrees of freedom through which a blade is coupled to its neighbors may be much smaller than the actual number of degrees of freedom accounted for in the blade itself. With the transfer matrix approach the cyclic nature of the system is taken into account by realizing that the state vector describing the behavior of each blade in an N-blade system is, at any given time, periodic with period N/n, where n is some integer.

The present work centers on the study of the localization phenomenon in a general, mono-coupled, mistuned cyclic assembly. The primary goal of the study is the development of a measure of sensitivity to mistuning. Such a measure would ideally identify regions of high sensitivity in the space of the design parameters, thereby predicting the risk of the occurrence of strong localization in various classes of bladed-disk assemblies. The work is based entirely on a transfer matrix formulation of a mono-coupled assembly.

The paper is organized as follows. In Section 2 the free dynamics of a general, mono-coupled, nearly cyclic structure are formulated with transfer matrices. Blade mistuning is introduced in the form of small, random parameters. For demonstrative purposes a blade assembly with two degrees of freedom per bay is introduced and used as an illustrative example for the remainder of the paper. Sections 3 and 4 contain, respectively, a study of the propagation of harmonic waves in, and of the natural modes of the tuned structure. In Section 5 we motivate the need for a sensitivity measure by illustrating the drastic effect that mistuning can have on the normal modes. Section 6 opens with a discussion of the effects of mistuning on the propagation of waves. The localization factor is subsequently defined as a means of quantifying localization. A measure of sensitivity is then suggested and analytical approximations of the localization factor are developed in terms of this sensitivity measure. The results are verified for the example system by Monte Carlo simulations. The main conclusions reached are given in Section 7.

The primary contribution of the paper is a method for estimating sensitivity to mistuning. This is accomplished through the definition of a sensitivity measure, whose inexpensive calculation is based on the model of a single bay in a mono-coupled assembly. Furthermore, a quantitative, universal relationship between the sensitivity measure and the localization factor verifies the appropriateness of the sensitivity measure.

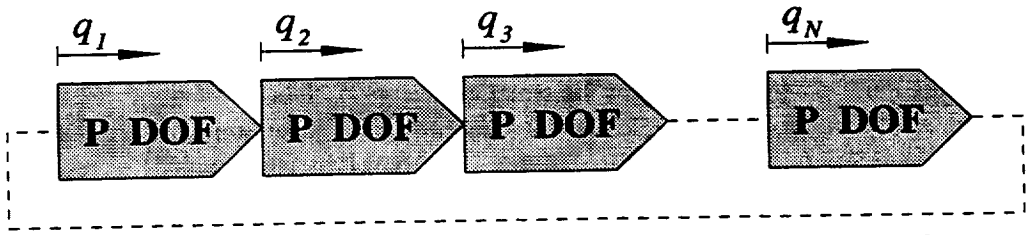

Figure 1 A general N-bay nearly cyclic assembly with P degrees of freedom per bay, *one* of which couples adjacent bays.

2. Transfer Matrices for Nearly Periodic, Mono-Coupled Structures.

The transfer matrix modeling of (nearly) periodic structures undergoing harmonic motion requires the definition of a state vector. For the discussion we introduce the terms *bay* and *interface*. A bay is exactly one spatial period in the periodic structure, such that only bays that are nearest neighbors are coupled. An interface is a point on the chain which separates two bays. To a state vector for a bay corresponds a transfer matrix that relates the states at two consecutive interfaces, or two consecutive bays. The dimension of the state vector must be twice the number of coupling coordinates at each interface [16]. A state vector is most commonly defined as the displacements of the coupling coordinates at an interface and the associated forces. For a mono-coupled structure (see Fig. 1) a two-by-two transfer matrix would relate the deflection and force at adjacent *interfaces*, thus:

$$\begin{bmatrix} q \\ F \end{bmatrix}_i = \hat{T}_0 \begin{bmatrix} q \\ F \end{bmatrix}_{i-1} \qquad i = 1, \ldots, N. \tag{1}$$

Where the subscript 0 implies a tuned system. Alternatively we could define a state vector *for a bay* as the deflections of the coupling coordinates at both ends of the bay (see Fig. 1). Then

$$\begin{bmatrix} q_{i+1} \\ q_i \end{bmatrix} = T_0 \begin{bmatrix} q_i \\ q_{i-1} \end{bmatrix} \qquad i = 1, \ldots, N \tag{2}$$

relates the states of two adjacent bays. This paper is based on the latter approach. The representation in Eq. (2) does not account for motion-independent external forces acting on the system and hence only the free dynamics are considered. The formulation of Eq. (2) requires two equations relating the coupling coordinates q_{i+1}, q_i and q_{i-1}. One is the equation of motion taken at interface i:

$$-q_{i+1} + \beta_o(\omega) q_i - q_{i-1} = 0, \qquad \beta_o(\omega) \in I\!R. \tag{3}$$

Note that Eq. (3) is symmetric in q_{i+1} and q_{i-1}, which requires the structure to be symmetric with respect to clockwise and counterclockwise numbering. This is the case only in the absence of aerodynamic and Coriolis forces. More on that later. The symmetry discussed here is different from Mead's [16] definition of symmetry of individual bays, and Eq. (3) holds for either symmetric or unsymmetric bays. Equation (3) does not account for dissipation since $\beta_o(\omega)$ is assumed to be real valued. The second equation in Eq. (2) is simply the identity $q_i = q_i$. Hence, each bay of a perfectly cyclic (tuned) mono-coupled structure, is described by the same transfer matrix representation

$$\begin{bmatrix} q_{i+1} \\ q_i \end{bmatrix} = \begin{bmatrix} \beta_o(\omega) & -1 \\ 1 & 0 \end{bmatrix} \begin{bmatrix} q_i \\ q_{i-1} \end{bmatrix} = T_0 \begin{bmatrix} q_i \\ q_{i-1} \end{bmatrix}, \qquad \beta_o(\omega) \in I\!R. \tag{4}$$

where Eq. (4) accounts for neither damping nor aerodynamic effects. In general each substructure possesses P degrees of freedom (see Fig. 1) and the generalized coordinates of the ith substructure are related to the coupling coordinate q_i through $P - 1$ equations of motion local to the bay. However, note that the coupling

degree of freedom has no special significance, and in fact we may choose any of the P degrees of freedom as our *reference* coordinate q_i. The choice must of course be the same for all bays.

When mistuning is introduced into the above cyclic system its periodicity is broken in one of two ways. First, the mistuning may be caused by a parameter which only appears in relation to the i^{th} interface, *e.g.*, the mistuning of parameters of individual blades. When this is the case the symmetry of Eq. (3) is unaffected and Eq. (4) is replaced by

$$\begin{bmatrix} q_{i+1} \\ q_i \end{bmatrix} = \begin{bmatrix} \beta(\delta_i) & -1 \\ 1 & 0 \end{bmatrix} \begin{bmatrix} q_i \\ q_{i-1} \end{bmatrix} = T_i \begin{bmatrix} q_i \\ q_{i-1} \end{bmatrix}, \quad i = 1, \ldots, N, \tag{5}$$

where δ_i is the small deviation (order ϵ or smaller) of the parameter from its average value, defining the mistuning for the i^{th} bay. This is a random variable of mean zero. In the notation, the frequency dependence of β has been dropped, for clarity.

Alternatively, the mistuning may be caused by a parameter which appears at both interfaces, i and $(i + 1)$, *e.g.*, the stiffness of a spring connecting two interfaces. Then Eq. (3) is no longer symmetric and Eq. (4) becomes

$$\begin{bmatrix} q_{i+1} \\ q_i \end{bmatrix} = \begin{bmatrix} \beta(\delta_i, \delta_{i-1}) & -\alpha(\delta_i, \delta_{i-1}) \\ 1 & 0 \end{bmatrix} \begin{bmatrix} q_i \\ q_{i-1} \end{bmatrix} = T_{i;i-1} \begin{bmatrix} q_i \\ q_{i-1} \end{bmatrix}, \quad i = 1, \ldots, N, \tag{6}$$

where δ_i and δ_{i-1} are random variables which correspond to the mistuned parameter *on each side* of interface i. Again, the frequency dependence of α and β is implied. Note the use of a semicolon in the index.

2.1. Example: A two-degree of freedom per bay model.

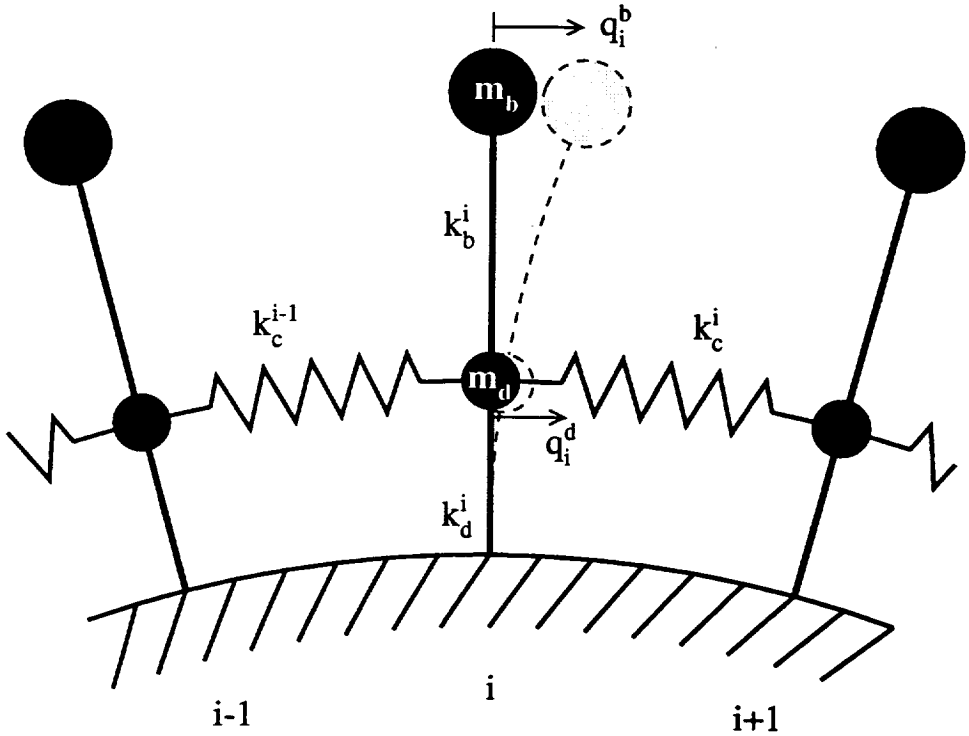

Figure 2 The i^{th} blade in an N-blade assembly with one blade coordinate and one disk coordinate per bay is shown with its two coupled neighboring blades.

Let us illustrate the above with an example. Consider the mono-coupled blade assembly with two degrees of freedom per bay shown in Fig. 2. Dye and Henry [3] were among the first to propose this blade assembly model and it has been used subsequently both for blade assemblies [1] and for large space reflectors [15]. This system will be utilized for demonstrative purposes for the remainder of the paper. In Fig. 2, q_i^b represents the single-mode motion of the blade and q_i^d accounts for the motion of the disk at the blade root. Corresponding to q_i^b are the blade (modal) mass m_b and (modal) stiffness k_b^i. The mass m_d simulates the effective mass of the blade root and the corresponding section of the disk. The stiffness k_d^i represents the basic stiffness of the rotor disk, whereas k_c^i provides disk coupling between neighboring blades. It is assumed that all bays have identical masses m_b and m_d and that the stiffnesses k_b^i, k_d^i, and k_c^i may differ from one bay to the next. This reduces complexity and provides adequate means of mistuning the natural frequencies of the individual bays. The average values of the stiffnesses are k_b, k_d, and k_c, respectively, and correspond to the stiffnesses in a tuned assembly. We aim to study how different combinations of stiffness and mass values affect the sensitivity of the system to mistuning and how the sensitivity differs when the blade stiffness, the disk stiffness, or the coupling spring stiffness are mistuned.

We now proceed to formulate a transfer matrix representation of the system in Fig. 2. Bay i is defined as the i^{th} blade-disk element, including the spring connecting it to blade $(i+1)$ (see Fig. 3). The i^{th} interface is the point where bay i and bay $(i-1)$ meet. All parameters of bay i except the spring stiffness appear solely in relation with the i^{th} interface, whereas k_c^i connects interfaces i and $i+1$. For that reason, a dynamic force equilibrium at interface i will include both k_c^i and k_c^{i-1}. This yields the equations of motion

$$m_b \ddot{q}_i^b + k_b^i \left(q_i^b - q_i^d\right) = 0, \tag{7}$$

$$k_c^{i-1}\left(q_i^d - q_{i-1}^d\right) + k_c^i\left(q_i^d - q_{i+1}^d\right) + k_d^i q_i^d + k_b^i\left(q_i^d - q_i^b\right) + m_d \ddot{q}_i^d = 0, \tag{8}$$

where Eq. (7) is local to the i^{th} blade. We write the mistuned stiffnesses as

$$k_d^i = k_d(1+\delta_i^d), \qquad k_b^i = k_b(1+\delta_i^b) \quad \text{and} \quad k_c^i = k_c(1+\delta_i^c), \tag{9}$$

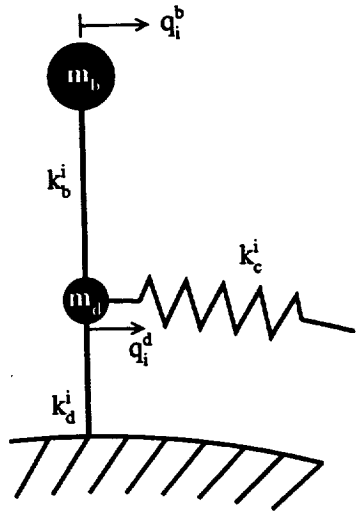

Figure 3 The i^{th} bay.

where δ_i^d, δ_i^c and δ_i^b are random variables with zero mean and standard deviation s_d, s_c and s_b, respectively. Assuming harmonic motion, $\ddot{q}_i^b = -\omega^2 q_i^b$, Eq. (7) may be rearranged as

$$q_i^d = \left(1 - \frac{m_b\omega^2}{k_b^i}\right) q_i^b = \left(1 - \frac{\bar{\omega}^2}{(1+\delta_i^b)}\right) q_i^b, \tag{10}$$

where

$$\bar{\omega}^2 = \frac{m_b\omega^2}{k_b} \tag{11}$$

is a dimensionless frequency. Equation (10) is now used to eliminate the blade coordinates from Eq. (8), which becomes,

$$q_{i+1}^d = \frac{1}{1+\delta_i^c}\left[2 + \delta_i^c + \delta_{i-1}^c + \frac{\bar{k}_d}{\bar{k}_c}(1+\delta_i^d) - \frac{\bar{\omega}^2(1+\delta_i^b)}{\bar{k}_c(1+\delta_i^b - \bar{\omega}^2)} - \frac{\bar{m}\bar{\omega}^2}{\bar{k}_c}\right] q_i^d - \frac{1+\delta_{i-1}^c}{1+\delta_i^c} q_{i-1}^d \tag{12}$$

where we have introduced the following dimensionless parameters

$$\bar{k}_d = \frac{k_d}{k_b} \qquad \bar{k}_c = \frac{k_c}{k_b} \qquad \bar{m} = \frac{m_d}{m_b}. \tag{13 a, b, c}$$

Defining

$$\beta_{i;i-1} = \frac{1}{1+\delta_i^c}\left[2 + \delta_i^c + \delta_{i-1}^c + \frac{\bar{k}_d}{\bar{k}_c}(1+\delta_i^d) - \frac{\bar{\omega}^2(1+\delta_i^b)}{\bar{k}_c(1+\delta_i^b-\bar{\omega}^2)} - \frac{\bar{m}\bar{\omega}^2}{\bar{k}_c}\right] \tag{14}$$

and

$$\alpha_{i;i-1} = \frac{1+\delta_{i-1}^c}{1+\delta_i^c} \tag{15}$$

we can write

$$\begin{bmatrix} q_{i+1}^d \\ q_i^d \end{bmatrix} = \begin{bmatrix} \beta_{i;i-1} & -\alpha_{i;i-1} \\ 1 & 0 \end{bmatrix} \begin{bmatrix} q_i^d \\ q_{i-1}^d \end{bmatrix}, \quad i = 1, \ldots, N, \tag{16}$$

where the state vector for the system in Fig. 2 consists of the disk generalized coordinates. Equation (16) corresponds to Eqs. (5) and (6). However, we note that only in the case of coupling spring mistuning, *i.e.*, $\delta_i^c \neq 0$, is the more complex form of Eq. (6) required, as otherwise $\alpha_{i;i-1} = 1$ and $\beta_{i;i-1} = \beta_i$. Thus, we have effectively formulated the dynamics of the system in terms of one reference degree of freedom per bay, in this case the coupling coordinate q_i^d. Since the system is only mono-coupled, the other coordinate (the blade degree of freedom) has been eliminated. Of course, once the state vector has been calculated via transfer matrix methods, the blade dynamics are recovered from Eq. (10).

In general, a mono-coupled assembly with P degrees of freedom per bay has $P-1$ equations local to the bay, such as Eq. (10), and a single equation relating coupling coordinates of adjacent bays, *e.g.*, Eq. (12). Needless to say, the complexity of this latter equation increases considerably as the number P is increased.

For a tuned assembly we have $\delta_i^c = \delta_i^d = \delta_i^b = 0$ and $\boldsymbol{T}_o$ has the form in Eq. (4), where β_o is given by

$$\beta_o = 2 + \frac{\bar{k}_d}{\bar{k}_c} - \frac{\bar{\omega}^2}{\bar{k}_c(1-\bar{\omega}^2)} - \frac{\bar{m}\bar{\omega}^2}{\bar{k}_c}. \tag{17}$$

In their work Cornwell and Bendiksen [15] and Bendiksen [1] took a different approach to the analysis of the same model. Using the theory of circulant matrices, they chose to eliminate the disk degrees of freedom by applying an approximate reduction procedure, arguing that in many cases of practical interest the disk stiffness is much greater than the blade stiffness. This is equivalent to setting $m_d = 0$ and thus $\bar{m} = 0$. We have found this to be an unnecessary approximation, although the approach allows one to evidence the coupling among *all* blades (as opposed to nearest neighbor coupling) through the disk degrees of freedom.

3. Propagation of Waves in the Tuned Structure.

We examine the propagation of waves in a general, mono-coupled, periodic structure whose dynamics are governed by Eq. (4). It has long been known that energy-carrying motions in periodic structures only occur in isolated frequency ranges known as "passbands." Outside the passbands only attenuated standing waves (or, more rarely, complex waves) can take place [16]. A physical understanding of these wave-propagation characteristics can be gained through the diagonalization of Eq. (4). This requires the solution of the eigenvalue problem:

$$\begin{bmatrix} q_{i+1} \\ q_i \end{bmatrix} = T_o \begin{bmatrix} q_i \\ q_{i-1} \end{bmatrix} = \lambda \begin{bmatrix} q_i \\ q_{i-1} \end{bmatrix}, \quad i = 1, \ldots, N. \tag{18}$$

Equation (18) yields the eigenvalues and eigenvectors of $\boldsymbol{T}_o$. Its significance is as follows. The eigenvectors of $\boldsymbol{T}_o$ define wave-modes, or characteristic waves, which propagate along the structure in such a way that the state-vector is multiplied by a complex scalar, λ, as the wave passes through each bay. Thus the eigenvalues,

$$\lambda_{1,2} = \frac{\beta_o}{2} \pm \sqrt{\left(\frac{\beta_o}{2}\right)^2 - 1}, \qquad \lambda_{1,2} \in \mathbb{C}, \beta_o \in \mathbb{R}, \tag{19}$$

define the frequency-dependent propagation properties of the corresponding wave-modes. The transfer matrix $\boldsymbol{T}_o$ in Eq. (4) is real with $\det \boldsymbol{T}_o = 1$, resulting in eigenvalues that are reciprocal and are either real or complex conjugates. We choose the convention that λ_1 has modulus greater than or equal to one. This associates λ_1 with the wave-mode traveling or attenuating in the direction of decreasing bay number. We shall call this direction the left or counterclockwise direction. The wave-modes appear as the eigenvectors, $[1, \lambda_2]^T$ and $[1, \lambda_1]^T$, corresponding to the eigenvalues λ_1 and λ_2, respectively. The condition $\lambda_1 \lambda_2 = 1$ indicates that the two wave-modes could also be written as $[\lambda_1, 1]^T$ and $[1, \lambda_1]^T$, which shows that they are equivalent except for their direction of travel. This is supported by the symmetry of the problem to clockwise or counterclockwise numbering of the bays. The independent wave-modes define the preferred means of wave propagation along the periodic assembly — much like normal modes are the preferred form of vibration of a structure. The normal modes form a basis for all vibration shapes in a structure. Similarly all possible waveforms in a structure may be written as a linear combination of the pair of wave-modes.

The eigenvectors of $\boldsymbol{T}_o$ are arranged as the columns of the matrix $\boldsymbol{X}$:

$$X = \begin{bmatrix} 1 & 1 \\ \lambda_2 & \lambda_1 \end{bmatrix}. \tag{20}$$

The matrix $\boldsymbol{X}$ defines the transformation

$$\begin{bmatrix} q_i \\ q_{i-1} \end{bmatrix} = X \begin{bmatrix} L \\ R \end{bmatrix}_i \tag{21}$$

from physical coordinates to left- and right-traveling wave coordinates at bay i, corresponding to the wave-mode basis. The displacement transfer matrix $\boldsymbol{T}_o$ thus is transformed into a diagonal wave transfer matrix as

$$\begin{bmatrix} L \\ R \end{bmatrix}_{i+1} = W_o \begin{bmatrix} L \\ R \end{bmatrix}_i = X^{-1} T_o X \begin{bmatrix} L \\ R \end{bmatrix}_i = \begin{bmatrix} \lambda_1 & 0 \\ 0 & \lambda_2 \end{bmatrix} \begin{bmatrix} L \\ R \end{bmatrix}_i. \tag{22}$$

Let $\lambda_1 = e^{\mu}$ define the complex *propagation constant*, μ, with $\mu = \gamma + j\sigma$. Here γ, the real part of the propagation constant, is the rate of exponential attenuation of the wave amplitude from one bay to the next. The imaginary part, σ, is the *interblade phase angle*, the difference in phase between the motion of adjacent bays. In the literature dealing with wave propagation in periodic systems [16] the interblade phase angle is usually called the *wave number*. The propagation constant contains all the information about the

frequency-dependent propagation of waves through the assembly. Since β_o in Eq. (19) is a real valued function of dimensionless frequency, $\bar{\omega}$, we distinguish between the following cases:

$|\beta_o(\bar{\omega})| < 2$ In this case λ_1 and λ_2 are complex conjugates of magnitude 1, yielding $\gamma = 0$. These frequencies define a *passband* in which waves travel without attenuation. From the real part of Eq. (19), the interblade phase angle is related to frequency by the dispersion relation:

$$2\cos\sigma = \beta_o(\bar{\omega}), \qquad 0 < \sigma < \pi. \tag{23}$$

For a given value of σ, Eq. (23) has as many frequency solutions as there are degrees of freedom in each bay [16]. Hence, the number of passbands equals the number of degrees of freedom in each bay. One can reason that the natural frequencies of the system will lie in the passband because a perfectly periodic system must have periodic modes. In the blade assembly literature [1-9] these modes are usually referred to as constant interblade phase angle modes, *i.e.*, modes with identical phase change from one bay to the next. The frequencies at which $\sigma = \pi/2$ will be referred to as *midband frequencies*. Note that the midband frequency is not necessarily located close to the mean frequency in the passband.

$|\beta_o(\bar{\omega})| > 2$ The eigenvalues are real, hence γ is nonzero, leading to attenuation. Also, adjacent bays are vibrating either in phase or out of phase, $\sigma = 0$ or $\sigma = \pi$, which implies that these are standing waves. These frequency ranges define *stopbands*.

$|\beta_o(\bar{\omega})| = 2$ This gives $\gamma = 0$ and $\sigma = 0$ or $\sigma = \pi$, and defines the bounding frequencies or the passband/-stopband edges.

3.1. Example.

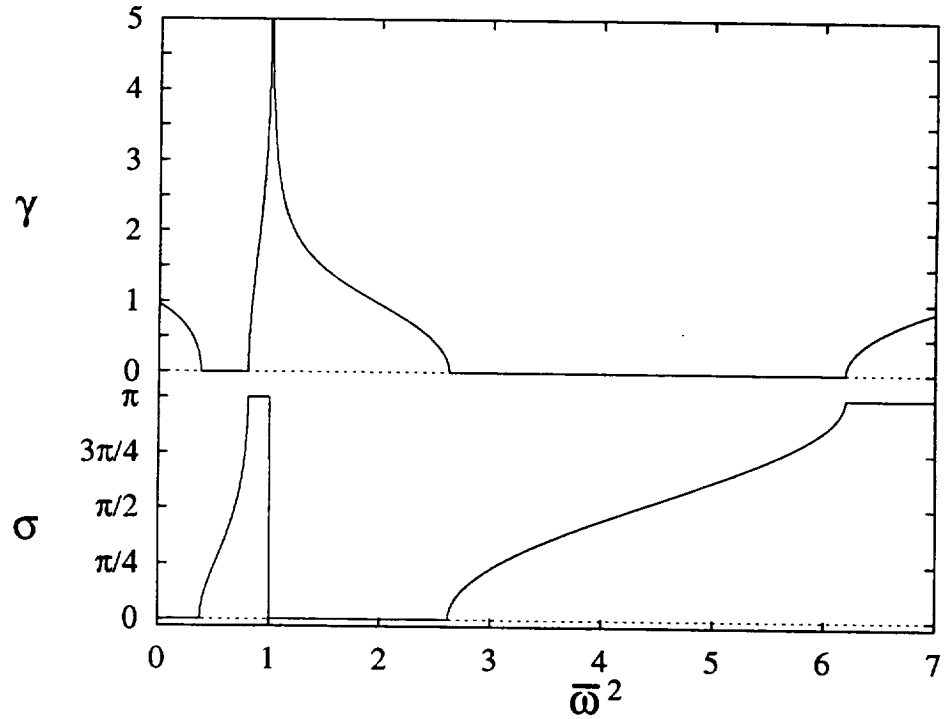

Figure 4 The passband/stopband structure of the assembly in Fig. 2, for $\bar{k}_c = \bar{k}_d = \bar{m} = 1$ (tuned case). Note the two distinct passbands where $\gamma = 0$. Also note a singularity at $\bar{\omega} = 1$, corresponding to the natural frequency of a cantilevered blade.

Figure 4 depicts the passband/stopband structure for the assembly in Fig. 2 for one set of parameter values. The rate of exponential attenuation, γ, and the interblade phase angle, σ, are displayed as a function of the dimensionless frequency. As predicted above, two frequency passbands are observed, corresponding to the two degrees of freedom per bay. In the passbands $\gamma = 0$ and unattenuated propagation of waves occurs. The wave travel is evidenced by the change of phase, $0 < \sigma < \pi$, from bay to bay. The other regions are stopbands, $\gamma \neq 0$, where standing waves decay exponentially. In stopbands, neighboring bays are either vibrating in phase or out of phase, hence there is no propagation. A special feature for this structure is the infinite attenuation observed at $\bar{\omega} = 1$, that is, at $\omega^2 = \frac{k_b}{m_b}$. We explain this behavior by pointing out that this is the natural frequency of a blade cantilevered at its root, hence at this frequency $q_i^d = 0$. Equation (10) confirms this. If the disk deflection equals zero, energy cannot be transmitted along the bays, hence the infinite attenuation of the waves, which can be viewed as an antiresonance.

4. Natural Frequencies and Mode Shapes of Finite Cyclic Systems.

We now make use of transfer matrices to derive a closed-form equation for the natural frequencies and normal modes of a finite, perfectly cyclic system. We already know from the theory of circulant matrices [17] that all cyclic structures share the same set of global modes, also referred to as constant interblade phase angle modes. We also know that structures described by real symmetric and circulant matrices have real eigenvalues, almost all of which are double. This is verified here using transfer matrices.

4.1. Natural Frequencies of a Tuned System

In searching for the natural frequencies of the system whose dynamics are described by Eq. (4), we recall that β_o is a function of frequency, $\bar{\omega}$. Using the cyclic nature of the N-bay system and Eq. (4), we obtain

$$\begin{bmatrix} q_2 \\ q_1 \end{bmatrix} = \begin{bmatrix} q_{N+2} \\ q_{N+1} \end{bmatrix} = {T_o}^N \begin{bmatrix} q_2 \\ q_1 \end{bmatrix}. \tag{24}$$

Hence nontrivial solutions are obtained if and only if

$$\det\left({T_o}^N - I\right) = 0. \tag{25}$$

Applying the appropriate transformation to $\boldsymbol{T}_o$ yields a Jordan canonical form $\boldsymbol{J}$. This allows for the case $\lambda_1 = \lambda_2 = 1$, which does not have a complete set of eigenvectors. Thus Eq. (25) transforms to

$$\det\left(J^N - I\right) = 0. \tag{26}$$

Since the matrix $\boldsymbol{J}$ is an upper triangular matrix with the eigenvalues λ_1 and λ_2 (from Eq. (19)) on the diagonal, $\boldsymbol{J}^N$ is also upper triangular with λ_1^N and λ_2^N on the diagonal. Hence Eq. (26) becomes

$$(\lambda_1^N - 1)(\lambda_2^N - 1) = 0, \tag{27}$$

or

$$\lambda_{1,2} = \sqrt[N]{1} = e^{j2\pi(n-1)/N} \qquad n = 1, \ldots, N. \tag{28}$$

Thus, from Eq. (19), the natural frequencies of the finite cyclic system, $\bar{\omega}_n$, satisfy

$$\frac{\beta_o(\bar{\omega}_n)}{2} \pm \sqrt{\left(\frac{\beta_o(\bar{\omega}_n)}{2}\right)^2 - 1} = e^{j2\pi(n-1)/N} \qquad n = 1, \ldots, N, \tag{29}$$

or

$$\beta_o(\bar{\omega}_n) = 2\cos\left(\frac{2\pi(n-1)}{N}\right) \qquad n = 1, \ldots, N. \tag{30}$$

For each n, the number of frequency solutions to Eq. (30) equals the number of degrees of freedom per bay, hence an N-bay assembly with P degrees-of-freedom per bay has NP natural frequencies. An important consequence of Eq. (30) is $\beta_o(\bar{\omega}_n) = \beta_o(\bar{\omega}_{N-n+2})$, *i.e.*, all natural frequencies are double, except $\bar{\omega}_1$ and, for a system with an even number of bays, $\bar{\omega}_{(N+2)/2}$. Note that the numbering scheme presented here does not place the natural frequencies in an ascending order. The relationship between the natural frequencies is: $\bar{\omega}_1 < \bar{\omega}_2 = \bar{\omega}_N < \bar{\omega}_3 = \bar{\omega}_{N-1} < \ldots < \bar{\omega}_{(N+1)/2} = \bar{\omega}_{(N+1)/2+1}$, if N is odd. If N is even the relationship is: $\bar{\omega}_1 < \bar{\omega}_2 = \bar{\omega}_N < \ldots < \bar{\omega}_{N/2} = \bar{\omega}_{N/2+2} < \bar{\omega}_{N/2+1}$, with unique frequency values at both ends. This pattern is repeated in each passband. The *passband edges* are natural frequencies for an N-blade system in the following cases. The lower passband edge is always a natural frequency corresponding to $n = 1$, or $\sigma = 0$. If and only if N is even is the upper edge a natural frequency, corresponding to $n = N/2$, or $\sigma = \pi$. Frequencies corresponding to all the other values of n are double. Furthermore, Eq. (30) gives $-2 \leq \beta_o(\bar{\omega}_n) \leq 2$, indicating that the natural frequencies lie in the system's passbands (see Eq. (23)). Thus, the assembly has N natural frequencies, mostly double, in each of its passbands.

At this point, let us digress to examine briefly what would be the effect of damping and that of aerodynamic coupling (limited to adjacent blades), hitherto excluded. Equation (4) would instead be

$$\begin{bmatrix} q_{i+1} \\ q_i \end{bmatrix} = \begin{bmatrix} \beta_o(\omega) & -\alpha_o(\omega) \\ 1 & 0 \end{bmatrix} \begin{bmatrix} q_i \\ q_{i-1} \end{bmatrix} = \tilde{T}_o \begin{bmatrix} q_i \\ q_{i-1} \end{bmatrix}, \qquad \beta_o(\omega), \alpha_o(\omega) \in \mathbb{C}. \tag{31}$$

The effect of damping is to render β_o complex, whereas aerodynamic terms cause β_o to be complex in addition to introducing the complex off-diagonal term α_o. The significance of α_o is that the system is no longer symmetric with respect to clockwise and counterclockwise numbering. This makes sense since wave propagation in the aerodynamic system depends on whether the direction of wave travel is the same as the direction of rotor rotation, or not. The eigenvalues of $\tilde{T}_o$ are then

$$\lambda_{1,2} = \frac{\beta_o}{2} \pm \sqrt{\left(\frac{\beta_o}{2}\right)^2 - \alpha_o}, \qquad \beta_o, \alpha_o \in \mathbb{C}, \tag{32}$$

instead of the values expressed in Eq. (19), with $\lambda_1 \lambda_2 = \alpha_o$. The fact that β_o is complex precludes the existence of passbands, as expected in a nonconservative system. Equation (30) for the natural frequencies takes on the more complicated form

$$\beta_o(\bar{\omega}_n) = e^{j2\pi(n-1)/N} + \alpha_o(\bar{\omega}_n) e^{-j2\pi(n-1)/N} \qquad n = 1 \ldots N, \tag{33}$$

indicating that the presence of α_o, which is due to aerodynamic terms, splits the natural frequencies of the system.

4.2. Nodal Diameter and Nodal Circle Modes.

From Eq. (30) there are N natural frequencies *in each passband* and we wish to determine the corresponding modes shapes. The *complex* mode shapes can be found simply through a recursive application of the wave modes given in Section 3. This yields the shape $[1, \lambda_{1,2}, \lambda_{1,2}^2, \ldots, \lambda_{1,2}^{N-1}]$, with $\lambda_{1,2}$ given by Eq. (28). The mode shape may also be given in terms of the interblade phase angle for the mode. A comparison of Eqs. (23) and (30) shows that to each $\bar{\omega}_n$* corresponds a mode shape with constant interblade phase angle σ_n, given by

$$\sigma_n = \frac{2\pi(n-1)}{N}, \qquad n = 1 \ldots N. \tag{34}$$

This result is independent of the passband number and implies that for a given n all frequency solutions of Eq. (30) are associated with the same *global* mode shape, characterized by a constant interblade phase angle

* Recall that the index n on natural frequencies does not imply an ascending ordering of natural frequencies.

along the assembly. By global we mean that modes of interblade phase angle σ_n, in the different passbands, feature the same deflection pattern from bay to bay along the assembly and differ only by their local vibration shape within an individual bay. In the first passband all blade-disk elements vibrate in their first mode, in the second passband in their second mode, *etc.* From Eq. (34) we note that $\exp(j\sigma_n) = \exp(-j\sigma_{(N+2-n)})$, which means that to each double natural frequency, $\bar{\omega}_n = \bar{\omega}_{(N+2-n)}$, corresponds a complex conjugate mode pair, one traveling clockwise and the other counterclockwise. Since they occur at the same frequency, these two traveling mode shapes may be combined to form two orthogonal *real* (standing waves) modes, simply by separating their real and imaginary parts.

The global modes are often classified in terms of their interblade phase angle. The first mode would thus be a zero interblade phase angle mode, with all bays moving in phase. The second mode and mode N are $\frac{2\pi}{N}$ interblade phase angle modes, *etc.* Another means of classification is to consider the number of *nodal diameters* featured by the mode. A nodal diameter is a term borrowed from continuous two-dimensional systems with cyclic symmetry, where it is a nodal line passing through the center of symmetry. In our case it is simply a diameter connecting pairs of nodes or bays with zero deflection positioned on opposite sides of the structure. The first mode is thus a zero nodal diameter mode. The second mode and mode N are one nodal diameter modes, *etc.* Another concept from continuous two-dimensional cyclic systems is that of *nodal circles*. Here, a nodal circle is drawn through the nodes of the individual bays of the assembly. Naturally in a cyclic system all N blades have nodes at the same distance from the center of the rotor. We use the number of these nodal circles to distinguish between modes with the same global shape but in different passbands. In general, in the first passband the blade-disk elements have no nodes, hence all modes in the first passband are zero nodal circle modes. In the second passband all blade-disk elements typically feature one node, hence all second passband modes are one nodal circle modes, and so on.

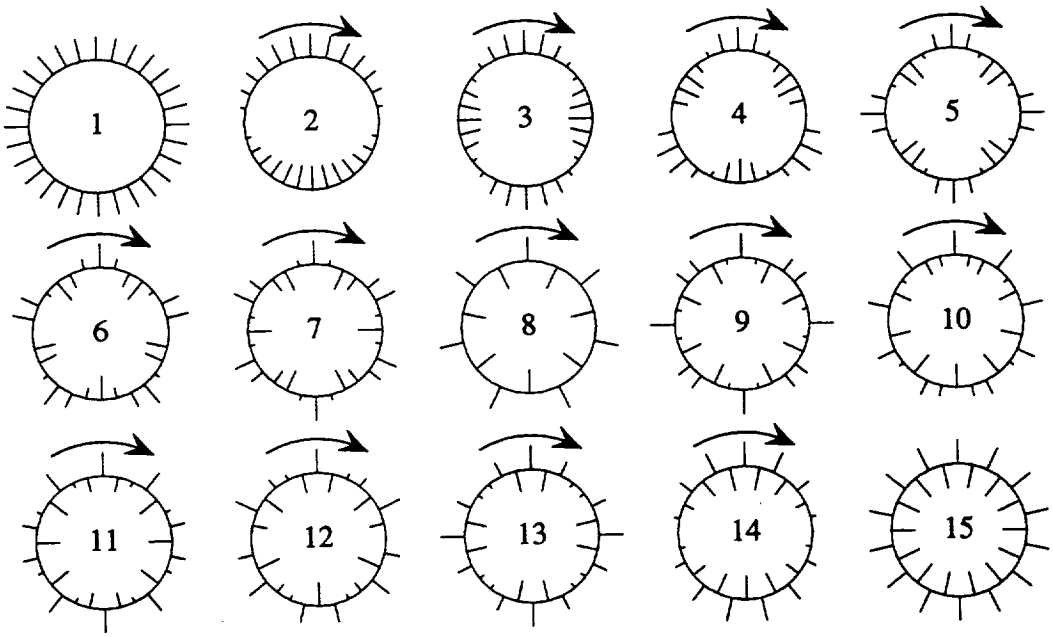

Figure 5 The global mode shapes of a 28-bay cyclic assembly. The 1st mode is a unique zero nodal diameter ($\sigma_1 = 0$) mode. The 2nd mode is a one nodal diameter ($\sigma_2 = \frac{\pi}{14}$) mode. The 28th mode (not shown) also has one nodal diameter but with $\sigma_{28} = -\frac{\pi}{14}$. The 15th mode is a fourteen nodal diameter ($\sigma_{15} = \pi$) mode and is unique.

Figure 5 illustrates the global modes of a 28-bay cyclic system. For modes corresponding to the same double natural frequency only one is shown. For example the 28th global mode would be like the 2nd global mode except for the direction of travel. Combining global modes 2 and 28 would yield two standing mode

shapes, identical to the one shown with one mode rotated 90 degrees with respect to the other.

4.3. Example.

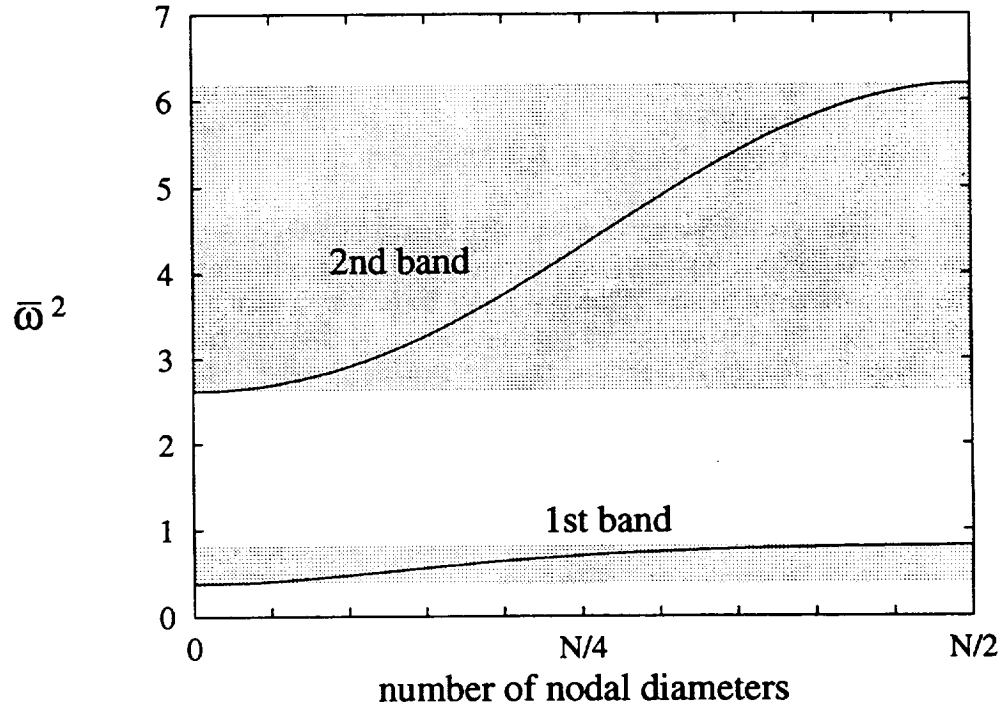

Figure 6 Natural frequencies as a function of the number of nodal diameters, for both passbands of the system in Fig. 2 with $\bar{k}_c = \bar{k}_d = \bar{m} = 1$.

Turning our attention to the system of Fig. 2, we have, from Eqs. (30) and (17)

$$\beta(\bar{\omega}_n) = 2 + \frac{\bar{k}_d}{\bar{k}_c} - \frac{\bar{\omega}_n^2}{\bar{k}_c(1-\bar{\omega}_n^2)} - \frac{\bar{m}\bar{\omega}_n^2}{\bar{k}_c} = 2\cos\left(\frac{2\pi(n-1)}{N}\right) \qquad n = 1, \ldots, N, \tag{35}$$

which when solved for $\bar{\omega}_n^2$ yields

$$\bar{\omega}_n^2 = \frac{2\bar{k}_c(1-\cos\sigma_n) + \bar{k}_d + \bar{m} + 1 \pm \sqrt{\left[2\bar{k}_c(1-\cos\sigma_n) + \bar{k}_d + \bar{m} + 1\right]^2 - 4\bar{m}\left[\bar{k}_d + 2\bar{k}_c(1-\cos\sigma_n)\right]}}{2\bar{m}}, \tag{36}$$

where the minus sign yields values in the first passband and the plus sign gives second passband frequencies. In Eq. (36), σ_n is the interblade phase angle of the n^{th} mode in the passband, given in Eq. (34).

It is customary to plot the natural frequency distribution against the number of modal diameters. This gives an indication of the number of natural frequencies per unit frequency, *the modal density*, in a given frequency range. In Figure 6 this is done for $\bar{m} = 1$, $\bar{k}_d = 1$ and $\bar{k}_c = 1$. An interesting feature, sometimes overlooked, is that the curves have local extrema at zero and $N/2$, hence the modal density is infinite at passband edges. The curves increase monotonically from 0 to $N/2$ and possess no other extrema.

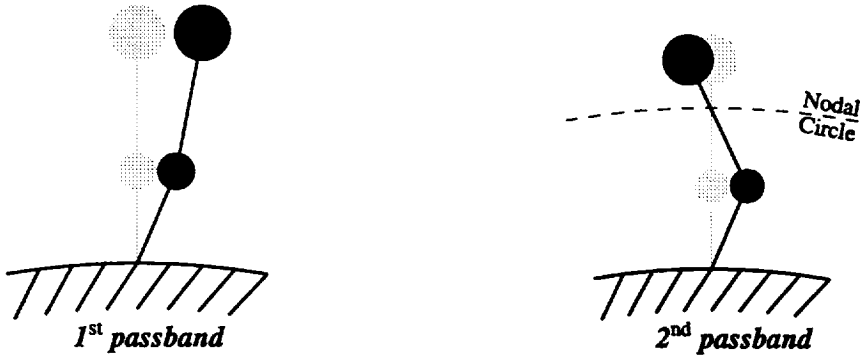

Figure 7 Typical local mode shapes in each passband with zero and one nodal circle, respectively.

While all circulant systems feature the same global mode shapes, illustrated in Fig. 5, the shape local to each bay is determined from Eq. (10), which may be used to calculate the radius of the nodal circle for the mode. For this system the modes of the first passband ($\bar{\omega}^2 < 1$) have no nodal circle (q^d and q^b have the same sign) and the modes of the second passband ($\bar{\omega}^2 > 1$) have one nodal circle (q^d and q^b have the opposite sign). From Eq. (10) we also see that the ratio between q^d and q^b is frequency dependent, hence the nodal radius varies within the passband. The local vibration patterns of the blade-disk elements are shown in Fig. 7 for the two passbands.

Appendix A contains a detailed discussion of the effect of the system parameters on the width and location of the two passbands. The main findings are that the lower passband edges correspond to a mode which has all blades vibrating in phase and thus to a system in which the blades are completely uncoupled. By that we mean that no interaction occurs between bays. Also, a system is called *weakly coupled* in some passband if the passband is narrow.

5. Natural Modes of a Mistuned Structure.

Let us begin the analysis of mistuned systems by examining the effect mistuning has on the natural frequencies and mode shapes. When mistuning is introduced, the system is no longer symmetric with respect to the clockwise and counterclockwise directions. This loss of cyclicity results in a splitting of the double natural frequencies, such that the system has P clusters of N distinct natural frequencies, where N is the number of blades and P is the number of degrees of freedom per bay. The clusters of frequencies correspond, approximately, to the passbands of the system's tuned counterpart, although they generally are wider. The corresponding mode shapes are standing waves that no longer possess the cyclic symmetry exhibited by the tuned system, where all blades vibrate with the same amplitude. Instead, the vibration energy may be concentrated in a handful of blades that have significantly larger deflection than the majority of blades. We refer to this phenomenon as mode localization.

As an example of the effect of random mistuning, we consider the mode shapes of the mistuned blade assembly model depicted in Fig. 2. Figure 8 displays the global blade-to-blade pattern of the mode shapes in the second frequency cluster of a 28-blade assembly, where the individual blades vibrate primarily in their second mode (see Fig. 7). High levels of localization are observed. The mode shapes have changed drastically compared to the tuned modes depicted in Fig. 5, and the vibration energy is no longer uniformly distributed along the rotor, but concentrated in as few as 5 blade-disk elements. This may result in a substantial increase in amplitudes and a potential decrease in fatigue life.

A compact characterization of the strength of localization and the prediction of high sensitivity to mistuning is the subject of the remainder of this study.

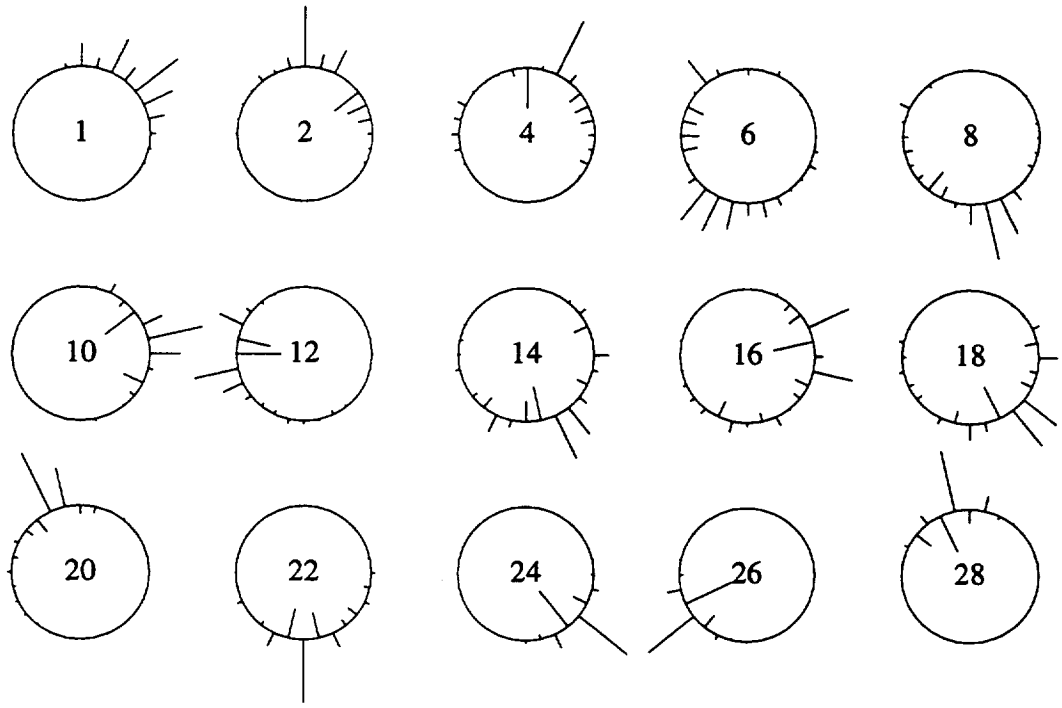

Figure 8 Localized modes in the second frequency cluster of a 28 blade assembly with $\bar{k}_d = \bar{m} = 1$, $\bar{k}_c = 0.1$, and uniform random mistuning in the blade stiffness with 5% standard deviation ($s_b = 0.05$). Modes are sorted by increasing natural frequency.

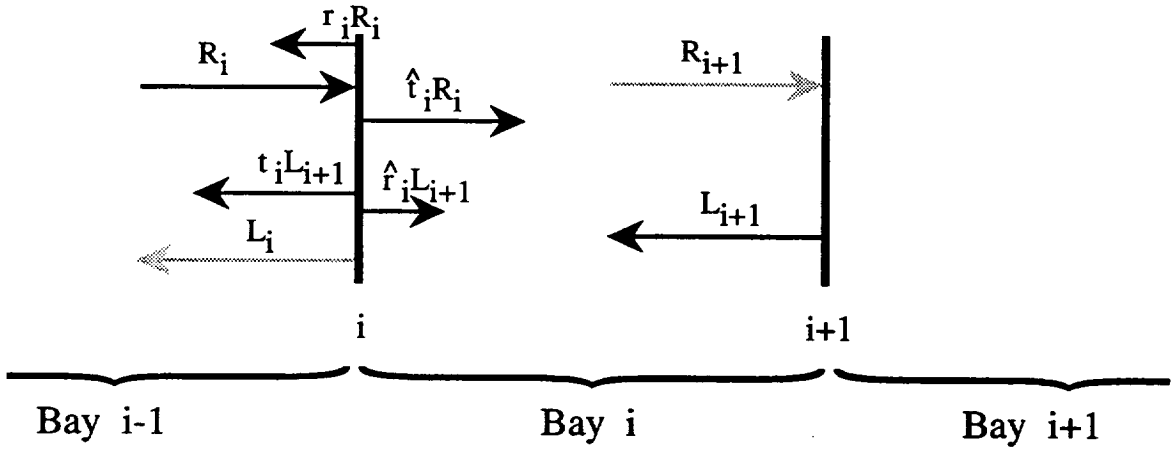

Figure 9 Scattering of waves at substructure interfaces.

6. Waves in Mistuned Systems.

A statistical approach is chosen to examine the high sensitivity to mistuning and the occurrence of localization in randomly mistuned assemblies. A statistical description of the modes of vibration is not practical due to the switching of the associated natural frequencies as the strength or the distribution of mistuning varies. We choose instead to examine the propagation of incident waves in mistuned assemblies. This allows us to control the frequency at which we wish to examine localization. In order to avoid the contamination of the localization effect by the cyclicity condition, an infinite assembly is studied. We further assume that mistuning is restricted to a segment of N bays (numbered from $i = 1$ to $i = N$) embedded in an otherwise

tuned infinite assembly. We are interested in the transmission of incident waves along the mistuned segment. An advantage of this approach is that a traveling wave that exits the mistuned segment will be propagated away and will not return.

In Section 3 we demonstrated how the transfer matrix $\boldsymbol{T}_o$ of a tuned bay is diagonalized by the similarity transformation defined by the matrix $\boldsymbol{X}$, which has as its columns the eigenvectors of $\boldsymbol{T}_o$. We called the diagonalized matrix a wave transfer matrix, $\boldsymbol{W}_o$. The transformation introduces a new set of coordinates, namely the left– and right-traveling components of a wave. The transformation defined by $\boldsymbol{X}$ does not, in general, diagonalize the transfer matrix of a bay belonging to the mistuned segment, $\boldsymbol{T}_i$ or $\boldsymbol{T}_{i;i-1}$ ($i = 1, \ldots, N$), as the case may be. Instead a non-diagonal wave transfer matrix is generated. The elements of this matrix may be expressed in terms of the more familiar reflection and transmission coefficients, as follows.

At the interface between dissimilar bays, waves are split into a transmitted part and a reflected part. As illustrated in Fig. 9, the left traveling wave incident to bay $i-1$, L_i, is the sum of a transmitted left traveling wave, $t_i L_{i+1}$ and a reflected right traveling wave, $r_i R_i$. Likewise, the right-traveling wave incident to bay $i+1$, R_{i+1}, is comprised of a transmitted part, $\hat{t}_i R_i$, and a reflected part, $\hat{r}_i L_{i+1}$. Here t_i and $\hat{t}_i$ are transmission coefficients and r_i and $\hat{r}_i$ are reflection coefficients in the left and right directions, respectively. Transmission and reflection coefficients are the complex amplitudes of transmitted and reflected waves due to an incident wave of unit amplitude, respectively. The above defines a scattering matrix, S_i:

$$\begin{bmatrix} L_i \\ R_{i+1} \end{bmatrix} = S_i \begin{bmatrix} R_i \\ L_{i+1} \end{bmatrix} = \begin{bmatrix} r_i & t_i \\ \hat{t}_i & \hat{r}_i \end{bmatrix} \begin{bmatrix} R_i \\ L_{i+1} \end{bmatrix}, \tag{37}$$

where directional symmetry in the absence of aerodynamic forces dictates that $\hat{t}_i = t_i$ and $\hat{r}_i = r_i$. Solving Eq. (37) for R_{i+1} and L_{i+1} yields

$$\begin{bmatrix} L \\ R \end{bmatrix}_{i+1} = W_i \begin{bmatrix} L \\ R \end{bmatrix}_i = \begin{bmatrix} \dfrac{1}{t_i} & \dfrac{-r_i}{t_i} \\ \dfrac{r_i}{t_i} & t_i - \dfrac{r_i^2}{t_i} \end{bmatrix} \begin{bmatrix} L \\ R \end{bmatrix}_i . \tag{38}$$

Equation (38) tells us that the off-diagonal elements in $\boldsymbol{W}_i$ govern what portion of a right or left traveling wave is reflected, thereby generating a wave in the opposite direction. The transmitted portion of the incident wave is determined from the first diagonal element in the wave transfer matrix. For a tuned bay $\boldsymbol{W}_i = \boldsymbol{W}_o$ is diagonal and there is no reflection at the interface. Hence $r_i = 0$ and the wave is fully transmitted. For a mistuned bay there is a reflection, or scattering at the interfaces between bays. A wave incident to a segment of randomly mistuned bays will experience multiple reflections whose effect may be to trap a wave near the incidence region. Only a frequency-dependent fraction of an incident wave is transmitted along to the far end of the mistuned segment. This effect is called *localization.* In a mistuned system passbands no longer exist since all waves are attenuated.

For a segment of N dissimilar bays the wave transfer matrix is the product of the random wave transfer matrices of the individual bays

$$\mathcal{W}_N = \prod_{i=1}^{N} W_i = \begin{bmatrix} \dfrac{1}{\tau_N} & \dfrac{-\rho_N}{\tau_N} \\ \dfrac{\rho_N}{\tau_N} & \tau_N - \dfrac{\rho_N^2}{\tau_N} \end{bmatrix} . \tag{39}$$

The one-one term, $1/\tau_N$, tells us which portion of an incident wave is transmitted to the far end of the mistuned segment. Obviously the behavior of the transmission coefficient for the mistuned segment, τ_N, governs the strength of the effects of mistuning and the resulting localization. We define the *localization factor* as

$$\gamma = \lim_{N \to \infty} \left[\frac{1}{N} \ln \left| \frac{1}{\tau_N} \right| \right], \tag{40}$$

implying that asymptotically, the ratio of emergent to incident wave decreases exponentially with an increasing number of bays, N. The localization factor, γ, defines the average exponential decay rate per bay and thus is a descriptor of the strength of localization. Assuming that the random variables δ_i ($i = 1 \ldots N$) from Eqs. (5) and (6) form an ergodic sequence, then the transmission coefficient, $\tau_N(\delta_1, \ldots, \delta_N)$, is also ergodic. Ergodicity implies that, with probability 1, the limit in Eq. (40) is equivalent to the ensemble average for a finite mistuned segment of length N:

$$\gamma = \left\langle \frac{1}{2N} \ln \left| \frac{1}{\tau_N} \right|^2 \right\rangle, \tag{41}$$

where $\langle\rangle$ denotes the expected value of a random variable.

The assumption that a cyclic structure is infinite is of course a limitation. It must be understood that this type of analysis is only applicable if the localization is strong enough that the vibration energy is confined to a sufficiently small region compared to the size of the assembly. For a nearly cyclic finite system this basically requires that the wave be adequately attenuated before reaching the incidence region again and thus interacting with other waves from the same source.

6.1. Sensitivity to Mistuning.

In general Eqs. (40) and (41) for the localization factor cannot be evaluated in closed form. However, analytical approximations are possible using perturbation methods, as follows.

We seek an expansion of $\frac{1}{\tau_N}$ in Eq. (40) in terms of the small mistuning parameter, δ_i (δ_i of order ϵ or smaller), thus treating the mistuned system as a perturbation of the tuned system. This is obtained through a Taylor expansion of the function $\beta(\delta_i)$ in Eq. (5):

$$\beta(\delta_i) = \beta_o + \beta'(0)\delta_i + O(\delta_i^2) \tag{42}$$

and subsequent expansion of τ_N and expansion and averaging of γ. The expansion in Eq. (42) must of course be uniform, *i.e.*, $\beta'(0)$ must be of order one (order ϵ^0) or smaller. However, if the expansion in Eq. (42) is nonuniform, *i.e.*, when $\beta'(0)$ is large (order ϵ^{-1} or larger) the technique breaks down. In this case the perturbation expansion is only valid for δ_i second order (order ϵ^2) or smaller. This breakdown indicates high sensitivity to mistuning and it is when the breakdown occurs (if it occurs) that systems have been seen to enter the realm of strong localization. This suggests the use of the first-order Taylor coefficient of $\beta(\delta_i)$ as a *measure of sensitivity to mistuning*:

$$S = \beta'(0) \tag{43}$$

A similar scenario may take place in the Taylor expansion of the transfer matrix in Eq. (6), albeit with four different first-order Taylor coefficients for α and β with respect to δ_i and δ_{i-1}. We do not formally define a sensitivity measure for this case.

When the sensitivity measure, $S = \beta'(0)$, becomes large the expansion in Eq. (42) is nonuniform, indicating a qualitative change in the assembly's dynamics, and other avenues must be explored. Note that in the passbands of the tuned system we have $-2 \leq \beta_o \leq 2$, but when S is large, $\beta(\delta_i)$ in Eq. (42) has the potential to become large for first-order mistuning in that frequency range. This suggests treating the off-diagonal terms in the transfer matrix of Eq. (5) as small perturbations compared to the large $\beta(\delta_i)$, thus yielding an alternative expansion for the high sensitivity case.

The two techniques outlined here, for the cases of normal and high sensitivity, are detailed in the following sections.

6.2. Classical Perturbation Method — Normal Sensitivity.

Consider the case where the expansion (42) is valid for first-order mistuning (δ_i of order ϵ), *i.e.*, when $S = \beta'(0)$ is not large (S of order one or smaller). We shall refer to this case as low or normal sensitivity. The much simpler case in Eq. (5) is treated first to better explain the technique. In Eq. (5), $\beta_i = \beta(\delta_i)$ depends only on one mistuned parameter, with $\beta(0) = \beta_o$ corresponding to the tuned case. A uniform expansion of T_i in the small mistuning parameter δ_i yields

$$\begin{aligned} T_i = \begin{bmatrix} \beta(\delta_i) & -1 \\ 1 & 0 \end{bmatrix} &= \begin{bmatrix} \beta_o & -1 \\ 1 & 0 \end{bmatrix} + \begin{bmatrix} \beta'(0) & 0 \\ 0 & 0 \end{bmatrix} \delta_i + \begin{bmatrix} \beta''(0) & 0 \\ 0 & 0 \end{bmatrix} \frac{\delta_i^2}{2} + \dots \\ &= T_O + T'\delta_i + T''\frac{\delta_i^2}{2} + \dots \end{aligned} \tag{44}$$

A transformation to wave coordinates is accomplished with the matrix of eigenvectors of T_o,

$$X = \begin{bmatrix} 1 & 1 \\ e^{-j\sigma} & e^{j\sigma} \end{bmatrix}, \tag{45}$$

where σ is defined in Eq. (23). Note that the analysis is limited to the tuned system's passband, since there is already large attenuation in the stopband. The wave transfer matrix is expanded as

$$\begin{aligned} W_i = X^{-1}T_iX &= W_O + W'\delta_i + W''\frac{\delta_i^2}{2} + \dots \\ &= \begin{bmatrix} e^{j\sigma} & 0 \\ 0 & e^{-j\sigma} \end{bmatrix} + \begin{bmatrix} e^{j\sigma} & 1 \\ -1 & e^{-j\sigma} \end{bmatrix} \frac{\delta_i\beta'(0)}{2j\sin\sigma} + \begin{bmatrix} e^{j\sigma} & 1 \\ -1 & e^{-j\sigma} \end{bmatrix} \frac{\delta_i^2\beta''(0)}{4j\sin\sigma} + \dots \end{aligned} \tag{46}$$

We need to evaluate the wave transfer matrix for a segment of N mistuned bays, each with its own random mistuning parameter δ_i. The random variables δ_i corresponding to each bay are considered independent and identically distributed, with zero mean and standard deviation s_δ. An assembly of N bays has the wave transfer matrix $\mathcal{W}_N$, which, when expanded to the second order in the δ_i's, becomes

$$\begin{aligned} \mathcal{W}_N &= \prod_{i=N}^{1} \left(W_O + \delta_i W' + \frac{\delta_i^2}{2} W'' \right) + O(\delta_i^3) \\ &= {W_O}^N + \sum_{i=1}^{N} W_O^{i-1} W' W_O^{N-i} \delta_i + \sum_{i=1}^{N} W_O^{i-1} W'' W_O^{N-i} \frac{\delta_i^2}{2} + \sum_{i=1}^{N} \sum_{\substack{j=1 \\ j \neq i}}^{N} R\delta_i\delta_j + O(\delta_i^3). \end{aligned} \tag{47}$$

The matrix $\boldsymbol{R}$ in Eq. (47) has a highly complex form, not evaluated since that entire term will vanish in the averaging process that follows, due to independence of the random variables δ_i, $(i = 1 \dots N)$. For an approximation of the localization factor, only the first diagonal element of $\mathcal{W}_N$, $w_{11}^N = \frac{1}{\tau_N}$, is needed. We have

$$\frac{1}{\tau_N} = e^{jN\sigma} \left[1 + \frac{\beta'(0)}{2j\sin\sigma} \sum_{i=1}^{N} \delta_i + \frac{\beta''(0)}{4j\sin\sigma} \sum_{i=1}^{N} \delta_i^2 \right] + O(\delta_i^3), \tag{48}$$

$$\left| \frac{1}{\tau_N} \right|^2 = \left[1 + \frac{\beta'(0)^2}{4\sin^2\sigma} \sum_{i=1}^{N} \delta_i \sum_{l=1}^{N} \delta_l \right] + O(\delta_i^3). \tag{49}$$

Since the δ_i's have zero mean and are independent, we have $\langle \delta_i\delta_j \rangle = 0$ for $j \neq i$ and $\langle \delta_i\delta_i \rangle = s_\delta^2$. Using the expansion $\log(1 + x) = x + O(x^2)$, we obtain the approximation of the localization factor, valid for low sensitivity,

$$\gamma = \left\langle \frac{1}{2N} \ln \left| \frac{1}{\tau_N} \right|^2 \right\rangle \simeq \frac{1}{2} \left(\frac{\beta'(0)s_\delta}{2\sin\sigma} \right)^2 = \frac{(S(\bar{\omega}))^2 s_\delta^2}{2(2 + \beta_o(\bar{\omega}))(2 - \beta_o(\bar{\omega}))}, \qquad O(S) \leq 1, \tag{50}$$

where S is the sensitivity measure defined in Eq. (43). Note that both S and β_o are functions of $\bar{\omega}$ and vary within the passband. The localization factor, γ, allows for localization effects to be characterized in a simple and compact way, without extensive simulations of mistuned systems. Note that Eq. (50) is general and applies to any mono-coupled mistuned assembly, as long as the mistuned parameter is not one that connects the two interfaces bounding the bay. It is of interest to note that the second-order Taylor coefficient, $\beta''(0)$, is cancelled from the derivation. According to Eq. (50), the onset of localization increases as the sensitivity measure squared. Also, to first order, the localization factor increases with the square of the mistuning standard deviation. The approximation of the localization factor becomes unbounded at frequencies which correspond to the edges of the passband of the tuned structure, $\beta_o = \pm 2$. This is reasonable, since at those frequencies the transformation matrix $\boldsymbol{X}$ (see Eq. (45)) is singular.

In order to obtain a quick estimate of the level of localization present in a system, it is advantageous to focus on the localization factor at the midband frequency. This frequency corresponds to the interblade phase angle $\sigma = \pi/2$, thus is the *median* natural frequency* of the tuned system. As seen in Appendix A, the midband frequency need not be located close to the mean frequency of the passband. One has, at midband,

$$\gamma_{mid} = \frac{S_{mid}^2 s_\delta^2}{8}. \tag{51}$$

which gives a good indication of the strength of localization effects in a "typical" mode of the system.

Let us now consider the case where a parameter common to two adjacent bays is disordered. In this case the transfer matrix has the general form in Eq. (6), where α and β are functions of two independent and identically distributed random variables, δ_i and δ_{i-1}. Assuming that β and α may be uniformly expanded in the small disorder parameters δ_i and δ_{i-1}, we find an expansion of $\boldsymbol{T}_{i,i-1}$:

$$\begin{aligned} T_{i;i-1} &= \begin{bmatrix} \beta(\delta_i,\delta_{i-1}) & -\alpha(\delta_i,\delta_{i-1}) \\ 1 & 0 \end{bmatrix} = \begin{bmatrix} \beta_o & -\alpha_o \\ 1 & 0 \end{bmatrix} + \begin{bmatrix} \beta_{,i-1} & -\alpha_{,i-1} \\ 0 & 0 \end{bmatrix}_{(0,0)} \delta_{i-1} \\ &+ \begin{bmatrix} \beta_{,i} & -\alpha_{,i} \\ 0 & 0 \end{bmatrix}_{(0,0)} \delta_i + \begin{bmatrix} \beta_{,(i-1)(i-1)} & -\alpha_{,(i-1)(i-1)} \\ 0 & 0 \end{bmatrix}_{(0,0)} \frac{\delta_{i-1}^2}{2} \\ &+ \begin{bmatrix} \beta_{,i(i-1)} & -\alpha_{,i(i-1)} \\ 0 & 0 \end{bmatrix}_{(0,0)} \delta_i\delta_{i-1} + \begin{bmatrix} \beta_{,ii} & -\alpha_{,ii} \\ 0 & 0 \end{bmatrix}_{(0,0)} \frac{\delta_i^2}{2} + \ldots \\ &= T_O + T_{,1}\delta_i + T_{,2}\delta_{i-1} + T_{,11}\frac{\delta_i^2}{2} + T_{,12}\delta_i\delta_j + T_{,22}\frac{\delta_{i-1}^2}{2} + \ldots, \end{aligned} \tag{52}$$

where the index notation $\boldsymbol{T}_{,1}$ and $\boldsymbol{T}_{,2}$ has been adopted to denote differentiation with respect to the first variable (δ_i) and the second variable (δ_{i-1}), respectively. A transformation to wave coordinates is accomplished using the matrix $\boldsymbol{X}$ from Eq. (45). The result is an expansion of the wave transfer matrix in the small disorder parameters δ_i and δ_{i-1}:

$$W_{i;i-1} = W_O + W_{,1}\delta_i + W_{,2}\delta_{i-1} + W_{,11}\frac{\delta_i^2}{2} + W_{,12}\delta_i\delta_{i-1} + W_{,22}\frac{\delta_{i-1}^2}{2} + \ldots \tag{53}$$

The wave transfer matrix of an N-bay segment is

$$\begin{aligned} \mathcal{W}_N &= W_{N;N-1}W_{N-1;N-2}\cdots W_{2;1}W_{1;0} \\ &\simeq \prod_{i=N}^{1}\left(W_O + W_{,1}\delta_i + W_{,2}\delta_{i-1} + W_{,11}\frac{\delta_i^2}{2} + W_{,12}\delta_i\delta_{i-1} + W_{,22}\frac{\delta_{i-1}^2}{2}\right). \end{aligned} \tag{54}$$

* $\sigma = \pi/2$ does not correspond to a natural frequency unless $N/4$ is an integer. Nonetheless, in each passband, the frequency corresponding to $\sigma = \pi/2$ (see Eq. (23)) will have an equal number of frequencies above and below it.

Carrying the product out to the second order in the δ's, the one-one term is found to be, after tedious algebra,

$$\tilde{w}_{11}^N = \frac{1}{\tau_N} \simeq e^{jN\sigma}\left[1 + e^{-j\sigma}\left(W_{,1} + W_{,2}\right)_{11}\sum_{i=1}^{N}\delta_i + e^{-2j\sigma}\left(W_{,2}\,W_{,1}\right)_{11}\sum_{i=1}^{N}\delta_i^2 \right.$$
$$\left. + e^{-j\sigma}\left(W_{,11} + W_{,22}\right)_{11}\sum_{i=1}^{N}\frac{\delta_i^2}{2}\right] = e^{jN\sigma}\left[1 + C_1\sum_{i=1}^{N}\delta_i + C_2\sum_{i=1}^{N}\delta_i^2\right], \quad C_1, C_2 \in \mathbb{C} \tag{55}$$

The tilde on $\tilde{w}_{11}^N$ underlines the fact that a few liberties have been taken, *i.e.*, we have ignored very complicated terms that we know will vanish in the averaging process at a later stage in the derivation. The term containing $\boldsymbol{W}_{,2}\,\boldsymbol{W}_{,1}$ appears due to the occurrence of the same random variable in two adjacent matrices. Next the magnitude of $\tilde{w}_{11}^N$ is evaluated:

$$|\tilde{w}_{11}^N|^2 = 1 + R_1\sum_{i=1}^{N}\delta_i + R_2\sum_{i=1}^{N}\delta_i^2 + O(\delta^3), \quad R_1, R_2 \in \mathbb{R}. \tag{56}$$

Due to the terms linear in δ, a second-order expansion of $\log|w_{11}^N|^2$ is required, that is, $\log(1+x) = x - x^2/2 + O(x^3)$. Dividing by $2N$ and taking the limit as $N \to \infty$ yields the localization factor, after substantial algebra:

$$\gamma = \lim_{N\to\infty}\frac{1}{2N}\log|w_{11}^N|^2$$
$$\simeq s_\delta^2\left[\frac{\left[\beta_{,1} + \beta_{,2} - (\alpha_{,1} + \alpha_{,2})\frac{\beta_o}{2}\right]^2}{8\sin^2\sigma} - \frac{\beta_{,1}\beta_{,2} - \beta_o\beta_{,2}\,\alpha_{,1}}{2} + \frac{\alpha_{,11} + \alpha_{,22}}{4} - \frac{(\alpha_{,1} + \alpha_{,2})^2}{8}\right], \tag{57}$$

where

$$\beta_{,1} = \left.\frac{\partial\beta(\delta_i, \delta_{i-1})}{\partial\delta_i}\right|_{(0,0)} \qquad \beta_{,2} = \left.\frac{\partial\beta(\delta_i, \delta_{i-1})}{\partial\delta_{i-1}}\right|_{(0,0)}$$
$$\alpha_{,1} = \left.\frac{\partial\alpha(\delta_i, \delta_{i-1})}{\partial\delta_i}\right|_{(0,0)} \qquad \alpha_{,2} = \left.\frac{\partial\alpha(\delta_i, \delta_{i-1})}{\partial\delta_{i-1}}\right|_{(0,0)} \tag{58}$$
$$\alpha_{,11} = \left.\frac{\partial^2\alpha(\delta_i, \delta_{i-1})}{\partial\delta_i^2}\right|_{(0,0)} \qquad \alpha_{,22} = \left.\frac{\partial^2\alpha(\delta_i, \delta_{i-1})}{\partial\delta_{i-1}^2}\right|_{(0,0)},$$

which reduces to the form of Eq. (50) for $\beta(\delta_i, \delta_{i-1}) = \beta(\delta_i)$ and $\alpha(\delta_i, \delta_{i-1}) = 1$. Finally, in the numerous cases where

$$\alpha(\delta_i, \delta_{i-1}) = \frac{f(\delta_{i-1})}{f(\delta_i)}, \tag{59}$$

Eq. (57) simplifies to

$$\gamma = s_\delta^2\left[\frac{[\beta_{,1} + \beta_{,2}]^2}{8\sin^2\sigma} + \frac{\beta_{,2}}{2}\left(\beta_o\frac{f'(0)}{f(0)} - \beta_{,1}\right) + \frac{1}{2}\left(\frac{f'(0)}{f(0)}\right)^2\right]. \tag{60}$$

At midband Eq. (60) reduces even further, to:

$$\gamma_{mid} = \frac{s_\delta^2}{8}\left([\beta_{mid,1} - \beta_{mid,2}]^2 + 4\left[\frac{f'_{mid}(0)}{f_{mid}(0)}\right]^2\right). \tag{61}$$

6.3. Modified Perturbation Method — High Sensitivity.

As suggested in Section 6.1 and observed in Section 6.2, the Classical Perturbation Method fails in the limit of high sensitivity, *i.e.*, when $S = \beta'(0)$ is large. Not only may this be seen by the failure of the Taylor expansion of β (Eq. (42)), but also by the fact that γ in Eq. (50) becomes large (order ϵ^{-1}) for S large, while it supposedly is a small perturbation of its zero value in the tuned system's passbands. The introduction of first-order mistuning in a system with strong sensitivity ($\beta'(0) \gg 1$) has the effect that in the passbands $\beta(\delta_i)$ becomes large[1]. This suggests the following modified perturbation scheme, where the off-diagonal terms are considered as the perturbation.

$$T_i = \begin{bmatrix} \beta(\delta_i) & -1 \\ 1 & 0 \end{bmatrix} = \begin{bmatrix} \beta(\delta_i) & 0 \\ 0 & 0 \end{bmatrix} + \begin{bmatrix} 0 & -1 \\ 1 & 0 \end{bmatrix} = \bar{T}_i + \Delta T. \tag{62}$$

A brief review of the equation of motion, Eq. (3), aids in a physical interpretation of the Modified Perturbation Method. The larger β becomes compared to 1, the less q_i is influenced by q_{i+1} and q_{i-1}. Consequently, in Eq. (62), a coupled system is treated as a perturbation of the uncoupled system. Since the modified unperturbed matrix $\bar{T}_i$ is already diagonal, there is no need for a wave coordinate transformation. Hence the physical coordinates are also *"wave coordinates*[2]*"* and $\bar{T}_i$ is a wave transfer matrix for the unperturbed structure. The wave transfer matrix for the perturbed, N-bay structure is then

$$\mathcal{W}^N = \prod_{i=N}^{1} T_i \approx \prod_{i=N}^{1} \bar{T}_i + \sum_{l=1}^{N} \left[\prod_{i=N}^{l-1} \bar{T}_i \Delta T \prod_{i=l-1}^{1} \bar{T}_i \right] = \begin{bmatrix} \prod_{i=N}^{1} \beta(\delta_i) & -\prod_{i=N}^{2} \beta(\delta_i) \\ \prod_{i=N-1}^{1} \beta(\delta_i) & 0 \end{bmatrix}, \tag{63}$$

where the product is expanded to the first order in the perturbation, ΔT. Due to the special form of ΔT all terms in the sum vanish except the first one and the last one. These terms become the off-diagonal terms in the matrix product and do not affect the transmission coefficient. Thus, in accordance with Eq. (41) the localization factor becomes

$$\gamma = \langle \ln |\beta(\delta)| \rangle = \int \ln |\beta(\delta)| \mathrm{pdf}_\delta(\delta) d\delta, \tag{64}$$

where $\langle\rangle$ denotes an average and $\mathrm{pdf}_\delta(\delta)$ is the probability density function of the random variable δ.

Next we attempt to express the localization factor in terms of the large sensitivity measure, $S = \beta'(0)$. Focusing on the midband frequency, where the interblade phase angle is $\sigma = \pi/2$ and $\beta(0) = 0$, the first-order approximation of β_{mid} for small δ is (assuming that the remainder of the expansion is uniform)

$$\beta_{mid}(\delta) \simeq S_{mid}\delta, \qquad O(S_{mid}) > 1. \tag{65}$$

Equation (64) may now be written as

$$\gamma_{mid} \simeq \ln |S_{mid}| + \int \ln |\delta| \mathrm{pdf}_\delta(\delta) d\delta, \tag{66}$$

which in the case of a uniform distribution, $\delta \in [-W, W] \equiv [-\sqrt{3}s_\delta, \sqrt{3}s_\delta]$, reduces further, to

$$\gamma_{mid} \simeq \ln |S_{mid}| + \ln(\sqrt{3}s_\delta) - 1, \qquad O(S_{mid}) > 1, \tag{67}$$

[1] Recall that in a tuned system's passband $-2 < \beta(0) < 2$.

[2] Since the unperturbed structure is uncoupled it does not actually transmit waves.

a remarkably simple and general characterization of localization in the high sensitivity case. Note that only the system sensitivity and the mistuning standard deviation are needed to evaluate γ. Also note that since S_{mid} is large, γ_{mid} is not first order but of order one, corresponding to a strong localization behavior. Pierre [14] examined a chain of single-degree of freedom oscillators, where $S = 1/R$, *i.e.*, the sensitivity is the inverse of the dimensionless coupling between oscillators. His result verifies Eq. (67).

In the limit of strong sensitivity, the Modified Perturbation Method treats a coupled system as a perturbation of an uncoupled, disordered system. This implies that the method is applicable only to weakly coupled assemblies and leads to an interpretation of sensitivity as an inverse of the coupling among bays. High sensitivity to mistuning has already been observed in systems with weakly coupled bays [14]. However, the definition of coupling in complicated multi-parameter systems is not always possible, whereas the evaluation of $S = \beta'(0)$ is straightforward.

Note that the results of this section are valid only in the cases where the mistuning is not common to adjacent bays as in Eq. (6). Since the systems of immediate interest to us do not exhibit strong localization when common parameters are disordered, this extension is not developed here.

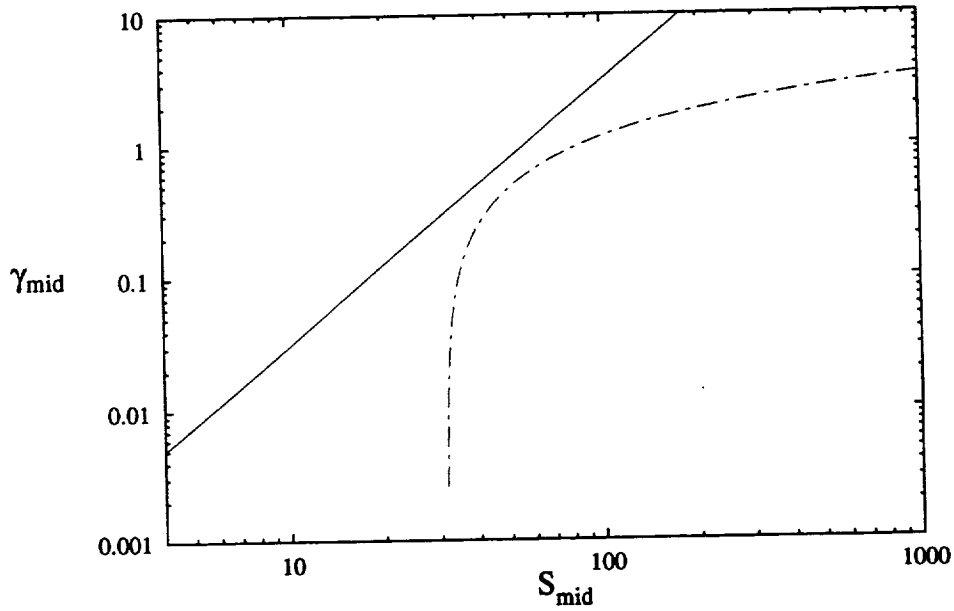

Figure 10 Approximation of the localization factor at the midband frequency as a function of the sensitivity measure ($S_{mid} = \beta'_{mid}(0)$). (———) corresponds to the classical perturbation result (Eq. (50)), valid for S_{mid} small. (— - —) corresponds to the modified approach (Eq. (67)), valid for S_{mid} large. The mistuning is uniform with 5% standard deviation.

Figure 10 illustrates the perturbation results for the mid-passband localization factor (Eqs. (51) and (67)) for a generic system described by Eq. (5), plotted as a function of sensitivity. The mistuning is uniform with 5% standard deviation. Equations (51) and (67) are valid in the limit of weak and strong sensitivity, respectively. Observe the rapid onset of localization, followed by a more moderate increase but large values of γ_{mid} in the limit of high sensitivity.

6.4. Example.

We now apply the tools developed above to the system depicted in Fig 2. Corresponding to the mistuned parameters k_b^i and k_d^i are measures of sensitivity to mistuning, S^{blade} and S^{disk}, according to Eq. (43). No such measure has been defined when the mistuned parameter is one connecting two interfaces, therefore the case where k_c is mistuned is given a different treatment. A parametric study identifies combinations of parameter values leading to high sensitivity. Analytical approximations of localization factors are obtained in the limits of weak and strong sensitivity. These approximations are verified by Monte Carlo simulations.

6.4.1. Measures of Sensitivity

Disk Mistuning: From the definition of β in Eq. (14), when $\delta_i^c = \delta_i^b = 0$, one has:

$$\beta(\delta_i^d) = 2 + \frac{\bar{k}_d}{\bar{k}_c}(1 + \delta_i^d) - \frac{\bar{\omega}^2}{\bar{k}_c(1 - \bar{\omega}^2)} - \frac{\bar{m}\bar{\omega}^2}{\bar{k}_c}. \tag{68}$$

Thus, from Eq. (43), the measure of sensitivity to disk stiffness mistuning is simply,

$$S^{disk} = \frac{k_d}{k_c} \tag{69}$$

Note that since $\beta(\delta_i^d)$ is linear with respect to the mistuning, its first-order Taylor expansion is exact. S^{disk} is easy to comprehend. The sensitivity increases linearly with the disk stiffness and is inversely proportional to the stiffness of the coupling spring. It is independent of the blade stiffness and the mass of the blade and the disk. The sensitivity measure is also independent of frequency and is therefore the same in both passbands. Note the obvious correlation between weak interblade coupling and high sensitivity as $k_c \to \infty$ and $k_d \to 0$. These results confirm those of Wei and Pierre [9], Pierre [14], and Cornwell and Bendiksen [15].

Blade Mistuning: For blade mistuning only, $\delta_i^d = \delta_i^c = 0$ and Eq. (14) simplifies to

$$\beta(\delta_i^b) = 2 + \frac{\bar{k}_d}{\bar{k}_c} - \frac{\bar{\omega}^2(1 + \delta_i^b)}{\bar{k}_c(1 + \delta_i^b - \bar{\omega}^2)} - \frac{\bar{m}\bar{\omega}^2}{\bar{k}_c} \tag{70}$$

Thus, from Eq. (43)

$$S^{blade} = \frac{\bar{\omega}^4}{(1 - \bar{\omega}^2)^2\bar{k}_c}. \tag{71}$$

Equation (71) is more complicated than it first would seem, because the location of the passbands, and hence the corresponding ranges for $\bar{\omega}$, depend on the system parameters $\bar{k}_c$, $\bar{k}_d$ and $\bar{m}$. The sensitivity is of course very different in the two passbands of the system. To give an example of how deceptive Eq. (71) is, one might *wrongly* assume that a large coupling spring stiffness, $\bar{k}_c$, always leads to low sensitivity. A counterexample is given below. However, small values of $\bar{k}_c$ do ensure high sensitivity, as we soon will see.

Focusing on the midband frequencies, we solve Eq. (35) for ω with $\sigma = \pi/2$, and obtain

$$\bar{\omega}^2_{mid} = \frac{2\bar{k}_c + \bar{k}_d + \bar{m} + 1}{2\bar{m}} \pm \frac{\sqrt{\left[2\bar{k}_c + \bar{k}_d + \bar{m} + 1\right]^2 - 4\bar{m}\left[\bar{k}_d + 2\bar{k}_c\right]}}{2\bar{m}}, \tag{72}$$

where the minus sign denotes the first passband. Substituting the values of $\bar{\omega}^2_{mid}$ into Eq. (71) yields

$$S^{blade}_{mid_{1,2}} = \frac{1}{4\bar{k}_c}\left[2\bar{k}_c + \bar{k}_d - \bar{m} - 1 \mp \sqrt{\left[2\bar{k}_c + \bar{k}_d + \bar{m} + 1\right]^2 - 4\bar{m}\left[\bar{k}_d + 2\bar{k}_c\right]}\right]^2, \tag{73}$$

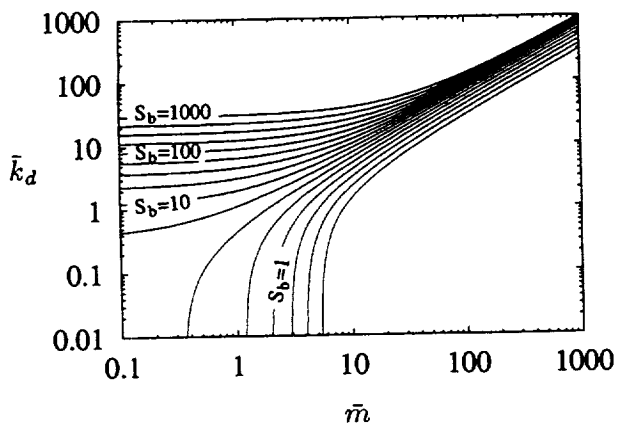

(a) $\bar{k}_c = 1$, *1st passband*

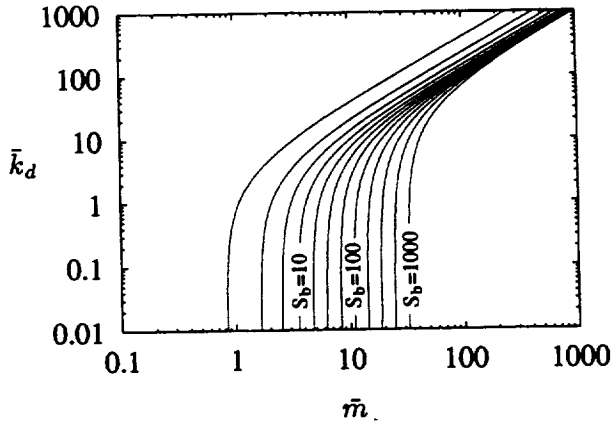

(b) $\bar{k}_c = 1$, *2nd passband*

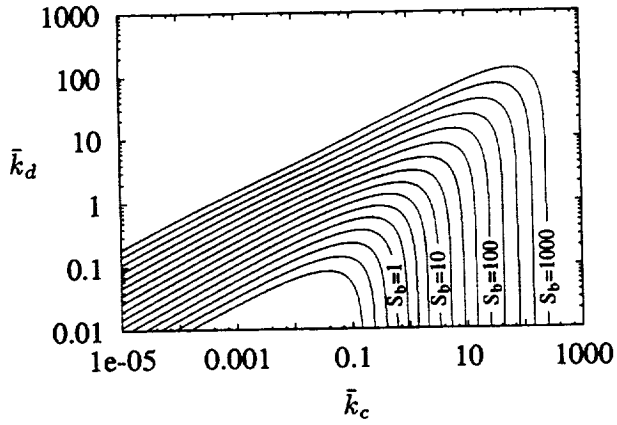

(c) $\bar{m} = 1$, *1st passband*

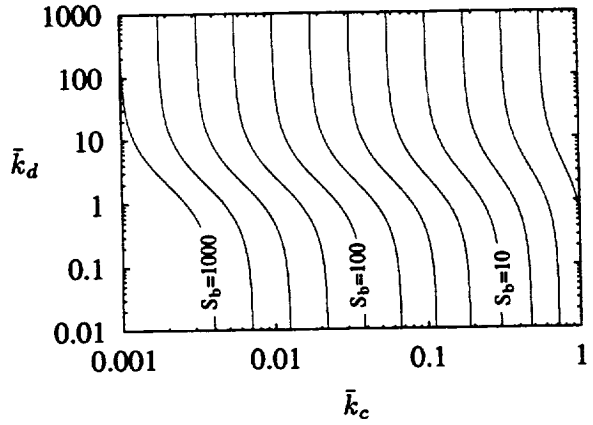

(d) $\bar{m} = 1$, *2nd passband*

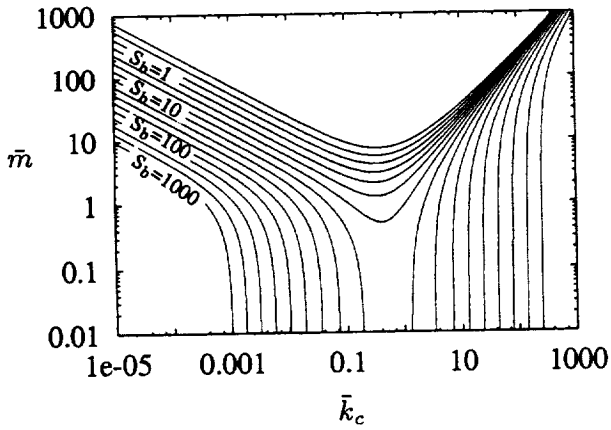

(e) $\bar{k}_d = 1$, *1st passband*

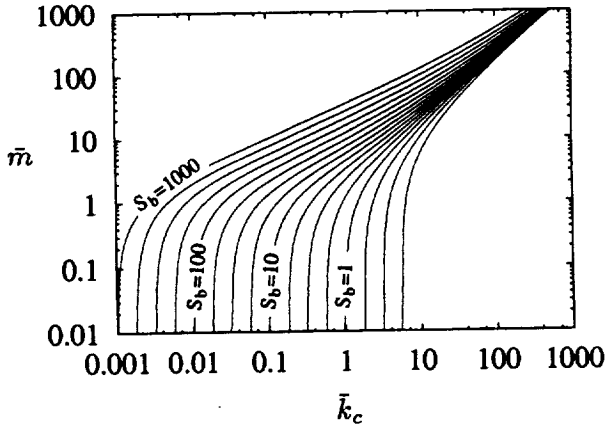

(f) $\bar{k}_d = 1$, *2nd passband*

Figure 11 Contours of the sensitivity measure, S_{mid}^{blade}, at the two passband centers. In each plot one of the parameters $\bar{k}_c$, $\bar{k}_d$ and $\bar{m}$ is fixed while the others are varied.

where the plus sign now corresponds to the first passband and the minus sign denotes second passband sensitivity. The sensitivity to blade mistuning at midband is plotted in Fig. 11. The plots show contours of the surface $S_{mid}^{blade}(\bar{k}_c, \bar{k}_d, \bar{m})$ by, in turn, fixing one parameter and varying the other two. A study of the plots yields information about the combination of parameter values that lead to strong sensitivity in the two passbands.

Figures 11(c) and 11(e) tell us that strong sensitivity in the first passband may be produced by large as well as small values of $\bar{k}_c$, the coupling spring stiffness. At first it seems surprising that a large $\bar{k}_c$ leads to high sensitivity at the first midband. Indeed, Fig. A2(c) in Appendix A indicates that for high values of $\bar{k}_c$ the passband width is large. However, we see that for large $\bar{k}_c$ all natural frequencies except the first one merge with the upper passband edge. Hence, although the passband is large, the range of the natural frequencies becomes small, and this system has very weak coupling. In Appendix A a system with stiff coupling springs is likened to a collection of blades mounted on the perimeter of a rigid ring. The blades are thus decoupled in the limit $\bar{k}_c \to \infty$, vibrating in their first mode with $q_i^d \simeq 0$. The opposite occurs in the second passband, where the bay is vibrating in its second mode that, unlike the first mode, requires a nonzero q_i^d. In this case the stiff coupling spring contributes heavily to the coupling between bays and the sensitivity decreases as $\bar{k}_c$ increases.

In addition to the above observations we note from Fig. 11 that if $\bar{m}$ is large enough, increasing it will cause a decrease in first passband sensitivity and an increase in second passband sensitivity. Varying $\bar{m}$ for small $\bar{m}$ has only a small effect on sensitivity, as evidenced by the lower portion of Fig. 11(e) and Fig. 11(f). Similarly we see that an increase in $\bar{k}_d$ increases first passband sensitivity except when $\bar{k}_d$ is small (Fig. 11(a)) or when $\bar{k}_c$ is very large (Fig. 11(c)). Second passband sensitivity decreases with increased $\bar{k}_d$ but only in ranges determined by $\bar{m}$ and $\bar{k}_c$. A combination of a small $\bar{k}_c$ and a large $\bar{k}_d$ leads to high sensitivity in both passbands.

Coupling Spring Mistuning: Although we have not defined a sensitivity measure for the system in Eq. (6), we attempt to examine its sensitivity to mistuning by considering all four possible first-order Taylor coefficients. From Eq. (14), with $\delta_i^d = \delta_i^b = 0$,

$$\beta(\delta_i^c, \delta_{i-1}^c) = \frac{1}{1+\delta_i^c}\left[\frac{\bar{k}_d}{\bar{k}_c} - \frac{\bar{m}\bar{\omega}^2}{\bar{k}_c} - \frac{\bar{\omega}^2}{\bar{k}_c(1-\bar{\omega}^2)} + 2 + \delta_i^c + \delta_{i-1}^c\right] = \frac{\beta_o + \delta_i^c + \delta_{i-1}^c}{1+\delta_i^c} \tag{74}$$

and from Eq. (15)

$$\alpha_{i;i-1} = \frac{1+\delta_{i-1}^c}{1+\delta_i^c} \tag{75}$$

from which

$$\left.\frac{\partial\beta(\delta_i^c, \delta_{i-1}^c)}{\partial\delta_i^c}\right|_{(0,0)} = 1 - \beta_o \qquad \left.\frac{\partial\beta(\delta_i^c, \delta_{i-1}^c)}{\partial\delta_{i-1}^c}\right|_{(0,0)} = 1 \tag{76}$$

and

$$\left.\frac{\partial\alpha(\delta_i^c, \delta_{i-1}^c)}{\partial\delta_i^c}\right|_{(0,0)} = -1 \qquad \left.\frac{\partial\alpha(\delta_i^c, \delta_{i-1}^c)}{\partial\delta_{i-1}^c}\right|_{(0,0)} = 1 \tag{77}$$

All four Taylor coefficients in Eqs. (76) and Eqs. (77) remain of order one or smaller for all parameter values. We conclude that in the case of coupling spring mistuning the classical perturbation is valid for all parameter values. This system is thus never strongly sensitive to coupling spring mistuning and only weak localization may be expected to occur.

6.4.2. Localization Factors and Monte Carlo Simulation.

Based on the expressions for the sensitivity measure, we are now in the position to examine the localization factor due to the above three types of disorder in the limits of low and high sensitivity. Using *Monte Carlo simulations* we confirm the validity of the perturbation approximations of the localization factor and the validity of S as a measure of sensitivity.

Monte Carlo simulations were performed in the following manner. A series of random transfer matrices representing the bays of a finite, cyclic assembly were generated, based on a random sequence, δ_i, from a random number generator. We labeled the resulting assembly one *realization* of mistuning. The matrices were multiplied together and transformed into wave coordinates, as explained in Section 6, yielding the wave transfer matrix for the mistuned assembly (see Eq. (39)). The localization factor for this particular realization of an N-bay system may be calculated from,

$$\gamma_N = \frac{1}{2N} \ln \left| \frac{1}{\tau_N} \right|^2 . \tag{78}$$

This was repeated for a large number of realizations of the assembly and the result averaged, adding realizations until the desired accuracy had been reached. The above constitutes one Monte Carlo simulation, for a system with some set of parameters $\bar{k}_c$, $\bar{k}_d$ and $\bar{m}$ vibrating at some frequency.

One point must be made about N, the number of bays in each realization. A product of a finite number of transfer matrices does not account for the infinite number of successive reflections that occur in the bays of an infinite system. A Monte Carlo simulation based on single bay realizations, $N = 1$, would only account for direct transmission through the bay and all reflections would be truncated. A Monte Carlo simulation using two bay realizations, $N = 2$, would additionally account for the wave fractions that are reflected twice as they propagate through the assembly, but all higher order reflections would be truncated, and so on. The number of bays in each realization is especially important when localization is strong (the off diagonal terms in $\boldsymbol{W}_i$ are no longer very small). For the cases studied, it was found that fewer than eight bays ($N = 8$) for each realization would, for strong localization, converge to an incorrect value for the localization factor. The number of realizations required for the convergence of γ_N varied but was usually in the thousands.

Verification by Monte Carlo simulations consists of two parts. On the one hand we verify the variation of γ as a function of frequency by running a series of simulations for a range of frequencies and plot the results along with the perturbation approximations in the passbands. The other part of the simulation process is the verification of the two perturbation solutions of γ_{mid} as a function of the sensitivity measure, S_{mid}. It is clear that both γ_{mid} and S_{mid} are functions of $\bar{k}_c$, $\bar{k}_d$ and $\bar{m}$ and may thus be parameterized with any or all of these parameters. This offers the opportunity to examine the *invariance* of the relationship between γ_{mid} and S_{mid} with respect to the system parameters, such that we would expect to obtain the same relationship no matter which of $\bar{k}_c$, $\bar{k}_d$ or $\bar{m}$ is varied. This relation should also be independent of which passband is chosen for the simulation. If this invariance is verified then the localization factor in Eqs. (51) and (67) will prove to be an extremely general tool for predicting mistuning effects when used in conjunction with the measure of sensitivity, S_{mid}.

For the Monte Carlo simulations a uniform distribution of width $2W$ was assumed for the mistuning. The standard deviation of the mistuning is $\frac{\sqrt{3}W}{3}$.

Disk Mistuning:

From the perturbation analysis, the localization factors are:

Weak Sensitivity

$$\gamma_d \simeq \frac{s_d^2 k_d^2}{8k_c^2 \sin^2 \sigma}, \tag{79}$$

$$\gamma_{d,mid} \simeq \frac{s_d^2 k_d^2}{8k_c^2}. \tag{80}$$

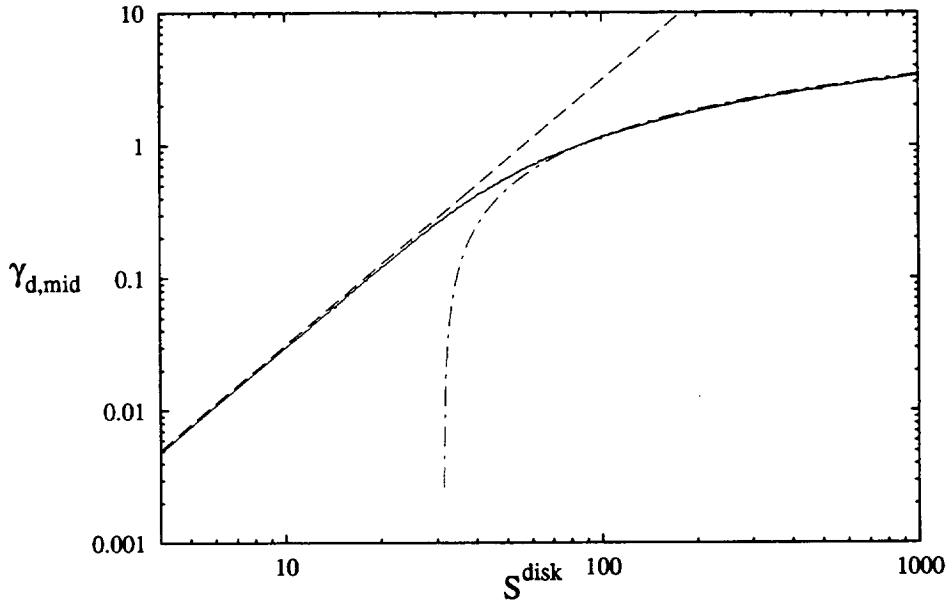

Figure 12 Monte Carlo simulations (———) are used to verify the invariance of Eq. (80) (— — -) and Eq. (82) (— · —) . The simulation result is a collection of data generated by varying both k_c and k_d in both passbands, with all results falling on the same curve. The standard deviation of uniform disk stiffness mistuning is 5%.

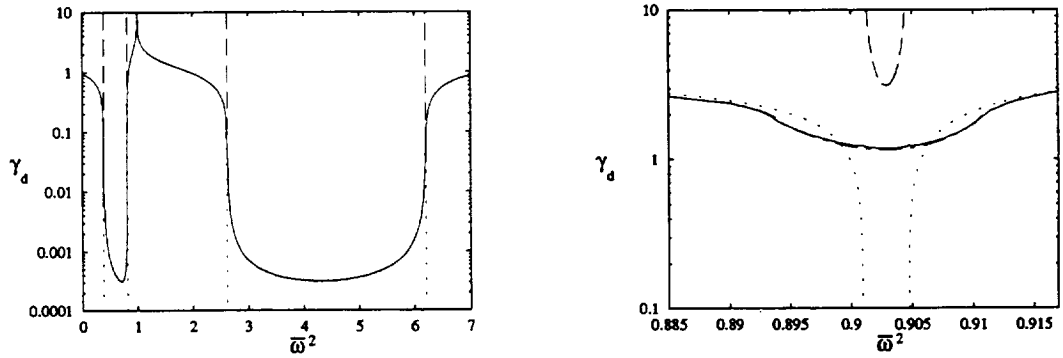

(a) $S^{disk} = 1$ (b) $S^{disk} = 100$ (1^{st} passband)

Figure 13 Exponential decay, γ_d, due to 5% disk stiffness mistuning *vs.* frequency. In stopbands Monte Carlo simulations (———) nearly coincide with the propagation constant for the tuned system (·····) . In (a) the simulations results overlap the classical perturbation result (— — -) , Eq. (79), in the passbands. In (b) the simulation agrees with the modified perturbation result (— · —) , Eq. (81).

Strong Sensitivity

$$\gamma_d \simeq \frac{k_c}{2\sqrt{3}s_d k_d}\left[(\beta(\sqrt{3}s_d)\ln|\beta(\sqrt{3}s_d)| - \beta(-\sqrt{3}s_d)\ln|\beta(-\sqrt{3}s_d)|\right] - 1, \tag{81}$$

$$\gamma_{d,mid} \simeq \ln\left|\frac{k_c}{k_d}\right| + \ln(\sqrt{3}s_d) - 1. \tag{82}$$

These results are plotted in Fig. 12 as a function of the sensitivity measure in Eq. (69), $S^{disk} = k_d/k_c$. Observe how the transition from the classical perturbation to the modified perturbation result, that is, from weak to strong localization, occurs at about the sensitivity value $S_{mid} \simeq 30$. Also note that the Monte Carlo results agree well with the perturbation results in the limits of strong and weak sensitivity. Figure 13 illustrates the validity of the perturbation approximations throughout the passbands. In Fig. 13(a) an excellent agreement between the simulation results and the classical perturbation solution is observed. Figure 13(b) demonstrates the quality of the modified perturbation solution in the passband of a very sensitive system, while the classical result grossly overpredicts the localization factor.

Blade Mistuning:

The perturbation analyses yield the following localization factors:

Weak Sensitivity

$$\gamma_b \simeq \frac{1}{\bar{k}_c^2}\left[\frac{\bar{\omega}^2}{(1-\bar{\omega}^2)}\right]^4 \frac{s_b^2}{8\sin^2\sigma} \tag{83}$$

$$\gamma_{b,mid} \simeq \frac{s_b^2}{128\bar{k}_c^2}\left[2\bar{k}_c + \bar{k}_d - \bar{m} - 1 \pm \sqrt{\left[2\bar{k}_c + \bar{k}_d + \bar{m} + 1\right]^2 - 4\bar{m}\left[\bar{k}_d + 2\bar{k}_c\right]}\right]^4 \tag{84}$$

where the plus and the minus signs denote the first and the second passband, respectively.

Strong Sensitivity

$$\gamma_b \simeq \frac{(1-\bar{\omega}^2)\beta_o \ln\left|\frac{\beta(\sqrt{3}s_b)}{\beta(-\sqrt{3}s_b)}\right|}{2\sqrt{3}s_b\left(\beta_o + \frac{\bar{\omega}^4}{\bar{k}_c(1-\bar{\omega}^2)}\right)} + \frac{\ln\left|\beta(\sqrt{3}s_b)\beta(-\sqrt{3}s_b)\right|}{2} - \frac{\bar{\omega}^4 \ln\left|\frac{1-\bar{\omega}^2+\sqrt{3}s_b}{1-\bar{\omega}^2-\sqrt{3}s_b}\right|}{2\bar{k}_c\sqrt{3}s_b\left(\beta_o + \frac{\bar{\omega}^4}{\bar{k}_c(1-\bar{\omega}^2)}\right)} \tag{85}$$

$$\gamma_{b,mid} \simeq \ln\left|\frac{1}{4\bar{k}_c}\left[2\bar{k}_c+\bar{k}_d-\bar{m}-1\pm\sqrt{\left[2\bar{k}_c+\bar{k}_d+\bar{m}+1\right]^2-4\bar{m}\left[\bar{k}_d+2\bar{k}_c\right]}\right]^2\right| + \ln(\sqrt{3}s_b) - 1 \tag{86}$$

with the same sign convention as above.

Figure 14 illustrates the transition from the classical perturbation approximation of the mid-band localization factor to the one obtained by the modified perturbation approach. The sensitivity measure, S_{mid}^{blade} (Eq. (73)), is affected by all parameters, $\bar{m}$, $\bar{k}_c$ and $\bar{k}_d$ as well as the passband number. Figure 14 contains three overlapping Monte Carlo simulation curves, each obtained by varying a different system parameter, *i.e.*, $\bar{m}$ in 1st passband, $\bar{k}_d$ in 2nd passband, and finally, $\bar{k}_c$ in 1st passband. These curves overlap nearly perfectly (except for a slight discrepancy at very high sensitivity) and they also agree closely with the corresponding simulation curve in Fig. 12 for disk stiffness mistuning. This suggests that $S = \beta'(0)$ is indeed highly suitable as a *universal* measure of sensitivity, at least for mono-coupled systems.

Figure 15 shows the exponential attenuation as a function of frequency in a system that has low sensitivity in the second passband but high first passband sensitivity. In the second passband the classical perturbation solution provides an excellent prediction of weak localization. In the first passband the modified perturbation approach matches the simulated results, thereby confirming the strong localization approximation.

Coupling Spring Mistuning:

Weak Sensitivity, from Eq. (60)

$$\gamma_c \simeq \frac{2-\beta_o}{2+\beta_o}\frac{s_c^2}{2} \tag{87}$$

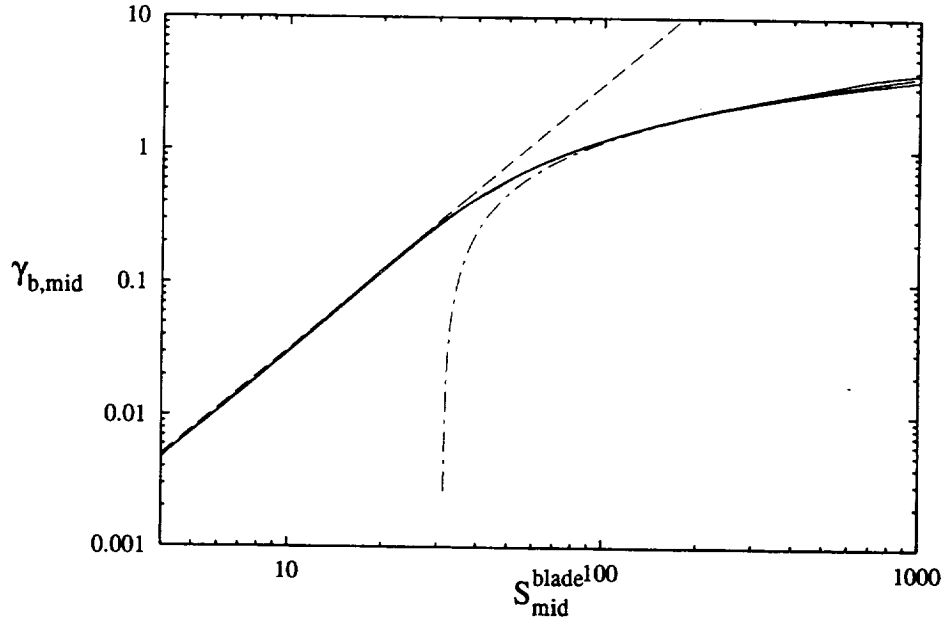

Figure 14 Monte Carlo simulations (———) are used to verify Eqs. (84) (— — —) and (86) (— · —). Multiple Monte Carlo simulations are obtained by varying $\bar{m}$ in 1st passband, $\bar{k}_d$ in 2nd passband and $\bar{k}_c$ in 1st passband. The standard deviation of blade stiffness mistuning is 5%. Note the near overlap of the various Monte Carlo results.

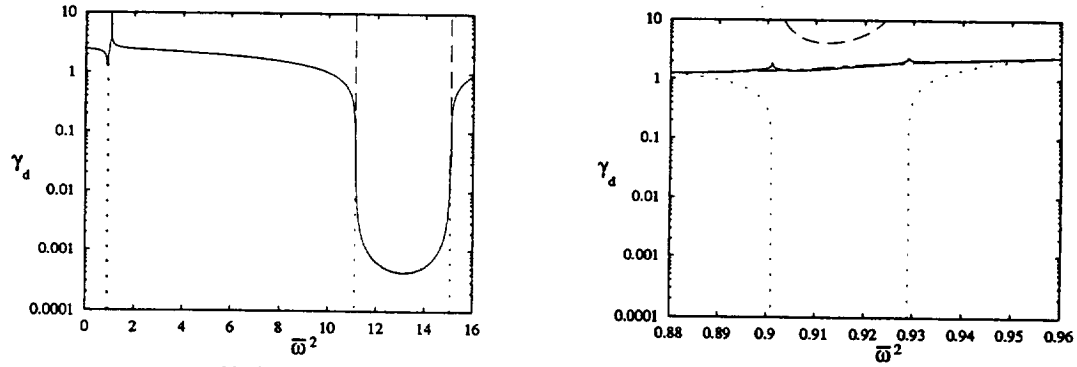

(a) $S^{blade}_{mid_2} \simeq 1.2$ (b) $S^{blade}_{mid_1} \simeq 123$ (1st passband)

Figure 15 Exponential decay, γ, due to 5% blade stiffness mistuning *vs.* frequency. In stopbands Monte Carlo simulations (———) agree with the propagation constant for the tuned system (· · · · · · ·). In (a) the simulations results overlap the classical perturbation result (— — —), Eq. (83), in the 2nd passband. In (b) the simulation agrees with the modified perturbation result (— · —), Eq. (85).

$$\gamma_{c,mid} \simeq \frac{s_c^2}{2} \tag{88}$$

Strong Sensitivity is never obtained through mistuning of $\bar{k}_c$.

In Fig. 16 we observe the excellent agreement between the classical perturbation result and the Monte Carlo simulations in the case of spring mistuning. This was evidenced for all other parameter values, which confirms the lack of high sensitivity to spring mistuning. It is interesting to note that the localization factor vanishes at the left passband edge. This is reasonable since at that frequency no stretching of the coupling

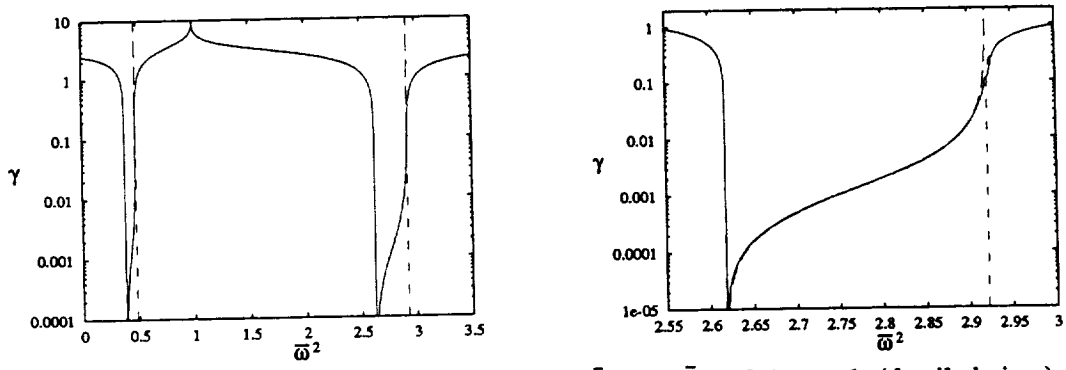

(a) $\bar{k}_d = 1.\ \bar{k}_c = 0.1\ \bar{m} = 1.$ (b) $\bar{k}_d = 1.\ \bar{k}_c = 0.1\ \bar{m} = 1.$ (detailed view)

Figure 16 Localization factor as a function of frequency in a system with coupling spring stiffness mistuning of standard deviation 5%. Results from Monte Carlo simulations (———) agree with the classical perturbation solution (— — —) in the passband and with the tuned system's propagation constant (- - -) in the stopbands. Note the lack of localization at the left passband edges and the very weak localization throughout the passbands.

spring occurs and mistuning of the spring stiffness is inconsequential.

6.4.3. Summary

We now sum up the results of this section and attempt to shed light on the meaning of the localization factor.

The system of Fig. 2 only exhibits low sensitivity to the mistuning of the coupling spring stiffness. This spared us the effort of developing a general expression for the localization factor in the case of mistuning of parameters connecting two interfaces. Although similar results may be expected for other blade assembly models, this should not be generalized to all periodic structures. A counterexample known to the authors is a nearly periodic beaded string [18], where mistuning the length of the string segments causes strong localization, even though the string connects two interfaces, similarly to the spring in Fig. 2.

Mistuning of either the disk stiffness or the blade stiffness can lead to strong localization. For disk stiffness mistuning we found high sensitivity as $k_c \to 0$ or $k_d \to \infty$. The sensitivity was independent of the blade stiffness, k_b, the masses m_d and m_b, and the frequency.

In the case of blade stiffness mistuning, all parameters $\bar{k}_c$, $\bar{k}_d$ and $\bar{m}$, as well as the frequency, were seen to affect the level of sensitivity. High sensitivity in the first passband was observed as $\bar{k}_d \to \infty$ and as $\bar{m} \to 0$ and for either $\bar{k}_c \to \infty$ or $\bar{k}_c \to 0$. In the second passband the system exhibits high sensitivity as $\bar{m} \to \infty$ and $\bar{k}_c \to \infty$, whereas $\bar{k}_d$ by itself cannot directly cause high sensitivity. However, lower values of $\bar{k}_d$ cause increased sensitivity in both passbands.

Figures 12 and 14 depict the transition from the classical to the modified perturbation approximation of γ in the interval $\gamma_{mid} \in [0.1, 1]$. We have used the subjective terms *weak* and *strong* to classify the localization in the two limits. According to Figs. 12 and 14 our classification would term $\gamma \leq 0.1$ as weak localization and $\gamma \geq 1$ as strong localization. In an infinite system with localization the vibration amplitude is governed by $e^{-\gamma N}$. Thus for $\gamma = 0.1$ the ratio of the amplitudes of adjacent bays is $e^{-0.1} \simeq 0.90$, such that on average the energy transmitted from one bay to the next is 82% and 56% is transmitted to the 3rd bay. For $\gamma = 1$ the average energy transmitted to the next bay is 13.5% and less than 0.25% of the energy reaches the 3rd bay! Of course, for the tuned, undamped system $\gamma = 0$ and 100% of the energy is transmitted.

The mistuned system whose modes are depicted in Fig. 8 has, at the second midband frequency, a sensitivity $S^{blade}_{mid_2} \simeq 25$. A quick check of Fig. 14 gives $\gamma_{mid} \simeq 0.2$. At $\gamma = 0.2$ the amplitude is decayed by 90% by the time it reaches bay number $-\ln|0.1|/0.2 = 11$. Of course the vibrations decay in both directions, clockwise and counterclockwise. Modes 14 and 16 in Fig. 8 are closest to the second midband and support this.

The significance of the value of γ depends on the total number of bays in the assembly. For example, $\gamma = 0.2$ indicates 90% attenuation over 11 bays and such localization would appear much less significant in a 10-bay assembly than it would in a 100-bay assembly. It would thus be useful to define a measure of localization that takes the total number of bays into consideration. This can be achieved by introducing the *localization length* or *localization scale*, $N^* = \frac{1}{\gamma}$, with which an alternative classification of localization could be the ratio $\frac{N}{N^*}$. In that case an N-bay assembly would experience 90% localization decay from one end to the other when $e^{-\frac{N}{N^*}} = 0.1$, or $\frac{N}{N^*} = 2.3$, from which the necessary value of γ (and thus S) could be obtained in terms of N. Higher values of $\frac{N}{N^*}$ would indicate more radical localization. The normalized inverse localization length, $\frac{N}{N^*}$, could be used as a simple predictive tool.

7. An Alternative Measure of Sensitivity.

Results of the preceeding sections indicate that high values of localization are associated with frequency ranges in which natural frequencies are closely packed. In Section 4.3 we introduced the concept of *modal density*, the number of natural frequencies per unit frequency. Here we examine the relationship between the modal density and localization as a source of an alternative measure of sensitivity.

Consider the eigenvalue problem:

$$\left\{C_o(\bar{\omega}_j) + \delta C(\bar{\omega}_j)\right\} \mathbf{u}_j = 0, \tag{89}$$

where $\boldsymbol{C}_o$ is a circulant matrix describing the dynamics of the full, tuned cyclic assembly and $\delta \boldsymbol{C}$ is a perturbation of that matrix due to mistuning of the system. $\boldsymbol{C}_o$ and $\delta \boldsymbol{C}$ are not transfer matrices. It may be shown that the first-order perturbation of the eigenvector, $\delta \mathbf{u}_j$, is inversely proportional to the distance between the corresponding tuned natural frequency, ω_j, and other tuned natural frequencies, ω_i, $i \neq j$ [13]. This confirms that if the natural frequencies of a system are closely spaced, the system will be highly sensitive to mistuning.

We attempt to develop a measure of sensitivity based on this information. An expression for the spacing of natural frequencies in the cyclic system in Eq. (4) is required. Solving Eq. (30) for n, the natural frequency number, and introducing a factor 2 to account for the fact that most natural frequencies are double yields

$$\frac{n(\bar{\omega})}{N} = 2\left[\frac{1}{2\pi}\cos^{-1}\left(\frac{\beta_o(\bar{\omega})}{2}\right) + \frac{1}{N}\right], \tag{90}$$

where n, a function of $\bar{\omega}$, is the number of natural frequencies smaller than $\bar{\omega}$. We define the ratio of the derivative of $n(\bar{\omega})$ to N as the modal density, $\eta(\bar{\omega})$, the relative number of modes per unit frequency, and obtain:

$$\eta(\bar{\omega}) = \frac{1}{N}\frac{\mathrm{d}n(\bar{\omega})}{\mathrm{d}\omega} = -\frac{\dfrac{\mathrm{d}\beta_o}{\mathrm{d}\bar{\omega}}}{2\pi \sin\sigma}. \tag{91}$$

The qualitative behavior of Eq. (91) is in some ways similar to that of the localization factor in Eq. (50), *e.g.*, near the passband edges ($\sigma \rightarrow 0$ or π) the modal density becomes large. However, we were not successful in establishing a quantitative relationship between γ and η. In the example we examine how correctly η predicts high sensitivity.

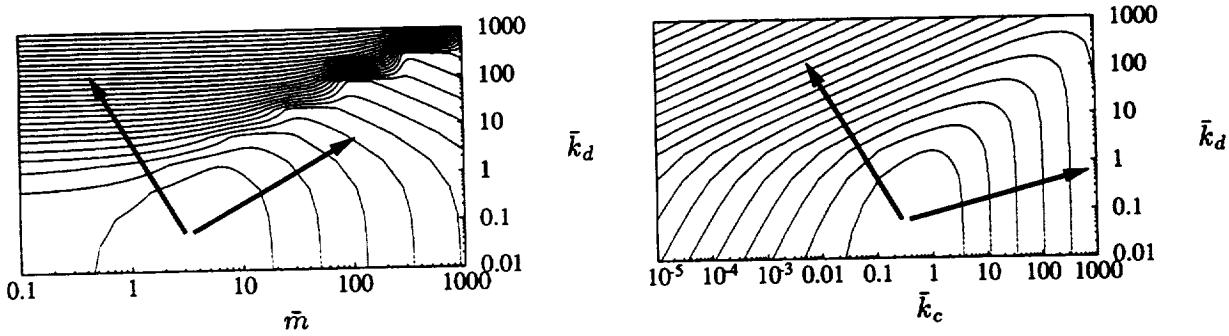

(a) $\bar{k}_c = 1$, *1st passband* (b) $\bar{m} = 1$, *1st passband*

Figure 17 Contours of η_{mid}, the modal density at midband (Eq. (93)) are plotted in the first passband by fixing one parameter and varying the other two. The arrows point in the direction of increasing values of η_{mid}.

Example:

From Eq. (91) we find the modal density of the system in Fig. 2 to be

$$\eta(\bar{\omega}) = \frac{2}{\pi \bar{k}_c} \frac{\bar{\omega}\left(\bar{m} + \frac{1}{(1-\bar{\omega}^2)^2}\right)}{\sqrt{4 - \left[2 + \frac{\bar{k}_d}{\bar{k}_c} - \frac{\bar{\omega}^2}{\bar{k}_c(1-\bar{\omega}^2)} - \frac{\bar{m}\bar{\omega}^2}{\bar{k}_c}\right]^2}}. \tag{92}$$

At mid-passband this simplifies to

$$\eta_{mid} = \frac{\bar{\omega}}{\pi \bar{k}_c}\left(\bar{m} + \frac{1}{(1-\bar{\omega}^2)^2}\right). \tag{93}$$

Figure 17 displays a parametric study of Eq. (93). Figure 17(b), in which $\bar{m}$ is held fixed in the first passband, confirms qualitative agreement with the equivalent study of the sensitivity measure S_{mid} in Fig. 11(c). A comparison of Fig. 17(a) and Fig. 11(a), in which $\bar{k}_c$ is fixed in the first passband, reveals a vital difference between the sensitivity measure, S_{mid}, and the modal density, η_{mid}. High values of $\bar{m}$ lead to high modal density, which should translate into high sensitivity to mistuning. This high modal density is verified by Fig. A2(a) in Appendix A. Figure 11(a), however, shows low sensitivity values for high values of $\bar{m}$. The Monte Carlo simulations verify that it is indeed the sensitivity measure, S, that correctly predicts low levels of localization in the first passband of systems with high values of $\bar{m}$. Although η correctly yields high values of the modal density, it fails to take into account the fact that all the frequencies of the first passband go to zero for high values of $\bar{m}$, and it is thus a poor predictor of sensitivity to mistuning in this case. We conclude that although the modal density is easily calculated and provides useful information regarding mistuning effects, it must be used with care.

8. Conclusion

A transfer matrix approach was suggested as an efficient way of modeling blade assemblies in which the coupling between remote blades is sufficiently weak to be ignored. We focused on mono-coupled assemblies, *i.e.*, assemblies in which only adjacent blade-disk sites are connected and only through one degree of freedom. All knowledge about the dynamics of tuned, mono-coupled assemblies is contained in a transfer matrix of dimension two, regardless of the actual number of degrees of freedom for each blade-disk element. We observed that the frequency domain is divided into *passbands*, in which waves propagate indefinitely, and *stopbands*, in which attenuated standing waves occur. We reasoned that the number of passbands is equal to the number of degrees of freedom for each blade-disk element and that the natural frequencies are contained in the passbands. The natural frequencies, mostly double, correspond to a pair of complex conjugate, constant interblade phase angle modes.

In the second part of the paper mistuning was seen to cause a splitting of the double natural frequencies and a drastic change in mode shapes. Instead of the extended modes possessed by the tuned system, the vibration energy concentrates in relatively few blades with amplitudes far beyond what was predicted by the tuned system analysis. These modes of a nearly cyclic system are a manifestation of *localization*, the effect of energy confinement due to scattering of waves at substructure interfaces.

We suggested a technique by which, based on the model of a single blade-disk element, the sensitivity of an assembly to mistuning could be expressed in terms of its parameters, using a sensitivity measure, S. The development of S was based on the qualitative changes observed in the system behavior as the expansion of the transfer matrix in the small mistuning parameter becomes nonuniform. Perturbation techniques were used to generate analytical approximations of the localization factor as a function of S in the limits of high and low sensitivity.

To validate the results, Monte Carlo simulations were performed on a popular model of a blade assembly. Our conclusion is that our measure of sensitivity, S, provides an excellent prediction of the levels of localization. Not only is the S measure simple, intuitive and cost-effective but also amazingly universal, *i.e.*, given a statistical distribution in the mistuning parameter, the relationship between γ_{mid} and S_{mid} is quantitatively the same, regardless of which parameter is mistuned, and is valid for a wide range of the system parameters. Approximations of the localization factor showed very good agreement with Monte Carlo simulations in the limits of high and low sensitivity, for all frequency values.

9. REFERENCES

[1] BENDIKSEN, O. O., 1984. *ASME Journal of Engineering for Gas Turbines and Power.* **106**(1), 25–33. "Flutter of Mistuned Turbomachinery Rotors.

[2] KIELB, R. E. and KAZA, K. R. V., 1984. *ASME Journal of Engineering for Gas Turbines and Power,* **106**(1), 17–24. "Effects of Structural Coupling on Mistuned Cascade Flutter and Response".

[3] DYE, R. C. and HENRY, T. A., 1969. *ASME Journal of Engineering for Power,* 182–188. "Vibration Amplitudes of Compressor Blades Resulting From Scatter in Blade Natural Frequencies".

[4] EL-BAYOUMY, L. E. and SRINIVASAN, A. V., 1975 *AIAA Journal,* **13**(4),460–464 "Influence of Mistuning on Rotor-Blade Vibrations".

[5] SRINIVASAN, A. V., 1984 *ASME Journal of Vibration, Acoustics, Stress and Reliability in Design,* **106**(2), 165–168. "Vibrations of Bladed-Disk Assemblies — A Selected Survey".

[6] EWINS, D. J. and HAN, Z. S. 1984. *Journal of Vibration, Acoustics, Stress and Reliability in Design,* **106** 211–217. "Resonant Vibration Levels of a Mistuned Bladed Disk".

[7] EWINS, D. J., 1973. *Journal of Mechanical Engineering Science,* **15**(3), 165–186. "Vibration Characteristics of Bladed Disc Assemblies".

[8] VALERO, N. A. and BENDIKSEN, O. O., 1986. *ASME Journal of Engineering for Gas Turbines and Power,* **108**(2), 293–299. "Vibration Characteristics of Mistuned Shrouded Blade Assemblies".

[9] WEI, S. T. and PIERRE, C., 1988. *ASME Journal of Vibration, Acoustics, Stress and Reliability in Design,* **110**(4), 429–438. "Localization Phenomena in Mistuned Assemblies With Cyclic Symmetry, Part I: Free Vibrations".

[10] KISSEL, G. J., 1987. *Ph.D. Dissertation, Massachusetts Institute of Technology.* "Localization in Disordered Periodic Structures".

[11] HODGES, C. H., 1982. *Journal of Sound and Vibration,* **82**(3), 411–424. "Confinement of Vibration by Structural Irregularity".

[12] HODGES, C. H. and WOODHOUSE, J., 1983. *Journal of Acoustical Society of America,* **74**(3), 894–905. "Vibration Isolation from Irregularity in a Nearly Periodic Structure: Theory and Measurements".

[13] PIERRE, C. and CHA, P.D. 1989. *AIAA Journal,* **27**(2), 227-241 "Strong Mode Localization in Nearly Periodic Disordered Structures"

[14] PIERRE. C., 1990. *Journal of Sound and Vibration.* **139**, 111–132. "Weak and strong vibration localization in disordered structures: a statistical investigation".

[15] CORNWELL, P. J. and BENDIKSEN, O. O., 1987. *AIAA Journal,* **27**(2), 219–226. "Localization of Vibrations in Large Space Reflectors".

[16] MEAD, D. J., 1975. *Journal of Sound and Vibration,* **40**, 1–18. "Wave Propagation and Natural Modes in Periodic Systems, I: Mono-Coupled Systems".

[17] DAVIS, P. J., 1979. *Circulant Matrices.* Wiley-Interscience

[18] ÓTTARSSON, G. S. and PIERRE, C., *Presentation of Invited Paper at the ASME Design Technical Conference Miami, FL, September 22-25, 1991.* "Vibration and Wave Localization in a Nearly Periodic Beaded String"

[19] ACHENBACH, J. D., 1973. *Wave Propagation in Elastic Solids.* Amsterdam: Elsevier Science Publishers.

[20] BRILLOUIN, L., 1953. *Wave Propagation in Periodic Structures.* New York: Dover.

[21] PESTEL, E. C. and LECKIE, F. A., 1963. *Matrix Methods in Elastomechanics.* New York: McGraw-Hill.

Appendix A: The Passbands of the 2-DOF Per Bay System: A Parametric Study

We examine the effect of the parameters $\bar{m}$, $\bar{k}_d$ and $\bar{k}_c$ on the passband/stopband structure of the tuned cyclic assembly and hence on the location of its natural frequencies. A physical interpretation of the passband edges may be given by recognizing the symmetries exhibited by a cyclic assembly vibrating at the bounding frequencies. These symmetries allow us to reduce the problem to that of single blade-disk elements. At the edge frequencies adjacent bays are vibrating in phase, $\sigma = 0$, or out of phase, $\sigma = \pi$. In the in-phase case, the coupling spring does no work and the assembly behaves as if the blades were uncoupled. This model, which we shall call the *free blade*, mimics the dynamics of the left, or lower, passband edges. In the out-of-phase case the midpoint of the coupling spring is stationary and the assembly behaves like a series of decoupled substructures, each connected to ground through two springs, each of stiffness $2\bar{k}_c$. We refer to this model as the *fixed blade*. It mimics an assembly vibrating at the right, or upper, passband edges. Note that the two models hold in both passbands.

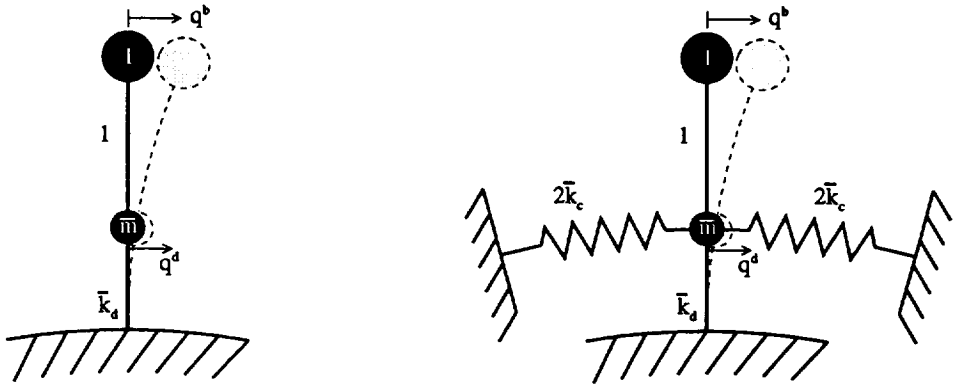

Figure A1 Single blade systems that mimic dynamic behavior at the passband edges. These systems are called the free blade system (left) and the fixed blade system (right).

These two single blade systems are illustrated in Fig. A1 and may be shown to have the natural frequencies

$$\bar{\omega}^2_{\text{free}_{1,2}} = \frac{(\bar{k}_d + \bar{m} + 1) \pm \sqrt{(\bar{k}_d + \bar{m} + 1)^2 - 4\bar{m}\bar{k}_d}}{2\bar{m}} \tag{A1}$$

for the free blade model and

$$\bar{\omega}^2_{\text{fixed}_{1,2}} = \frac{(\bar{k}_d + \bar{m} + 4\bar{k}_c + 1) \pm \sqrt{(\bar{k}_d + \bar{m} + 4\bar{k}_c + 1)^2 - 4\bar{m}(\bar{k}_d + 4\bar{k}_c)}}{2\bar{m}} \tag{A2}$$

for the fixed blade model. In both cases the minus sign corresponds to the first passband and the plus sign to the second band.

These single blade systems may be used to examine how the individual parameters affect the passband/stopband structure of the cyclic assembly. The results are summarized in table A1. The first, and most obvious point to be made is that the dimensionless parameter $\bar{k}_c$ has no effect on the lower passband edges. In the case of a low $\bar{k}_c$ the upper passband edges approach the lower edges, *i.e.*, the passbands narrow and vanish as $\bar{k}_c \to 0$, as seen in table A1. Less trivial is the case when $\bar{k}_c$ tends to infinity. The first passband motion of the fixed blade system is that of a blade cantilevered at its root with $\bar{\omega} = 1$. In the second mode of the fixed blade system the disk displacement must be nonzero. Hence as $\bar{k}_c \to \infty$ the corresponding natural frequency tends to infinity.

For vanishing disk stiffness $\bar{k}_d$, the free blade system behaves like a two-mass body free in space. The first mode of this system is a rigid body mode and hence the first passband begins at $\bar{\omega} = 0$. The second

natural frequency of the free blade system is $\bar{\omega}^2 = (1 + \bar{m})/\bar{m}$. The two natural frequencies of the fixed system when the disk is not present are

$$\bar{\omega}^2_{\text{fixed}_{1,2}^{(k_d=0)}} = \frac{(\bar{m} + 4\bar{k}_c + 1) \pm \sqrt{(\bar{m} + 4\bar{k}_c + 1)^2 - 16\bar{m}\bar{k}_c}}{2\bar{m}}, \quad \text{for} \quad k_d = 0. \tag{A3}$$

When $\bar{k}_d$ becomes infinite the substructures of the system becomes weakly coupled as evidenced by the vanishing of the passbands (see table A1). The spring stiffness $\bar{k}_c$ is obviously immaterial in this case and the first natural frequency of both the fixed blade and free blade systems approaches the blade natural frequency, $\bar{\omega} = 1$. As in the case of infinite coupling spring stiffness, the high stiffness of the disk degree of freedom leads to natural frequencies in the second passband that tend to infinity.

	1st passband		2nd passband	
	left edge	right edge	left edge	right edge
$\bar{k}_c \to 0$	$\bar{\omega}^2_{\text{free}_1}$		$\bar{\omega}^2_{\text{free}_2}$	
$\bar{k}_c \to \infty$	$\bar{\omega}^2_{\text{free}_1}$	1	$\bar{\omega}^2_{\text{free}_2}$	∞
$\bar{k}_d \to 0$	0	$\bar{\omega}^2_{\text{fixed}_1^{(k_d=0)}}$	$\frac{1+\bar{m}}{\bar{m}}$	$\bar{\omega}^2_{\text{fixed}_2^{(k_d=0)}}$
$\bar{k}_d \to \infty$	1		∞	
$\bar{m} \to 0$	$\frac{\bar{k}_d}{\bar{k}_d+1}$	$\frac{\bar{k}_d+4\bar{k}_c}{\bar{k}_d+4\bar{k}_c+1}$	∞	
$\bar{m} \to \infty$	0		1	

Table A1 Passband edges for limiting values of the assembly parameters. The values of $\bar{\omega}_{\text{free}_1}$ and $\bar{\omega}_{\text{free}_2}$ are given by Eq. (A1) and those of $\bar{\omega}_{\text{fixed}_1^{(k_d=0)}}$ and $\bar{\omega}_{\text{fixed}_2^{(k_d=0)}}$ by Eq. (A3).

Finally, the effect of the mass ratio $\bar{m}$ is examined. When $\bar{m} \to 0$ the mass of the disk is negligible relative that of the blade. The effective inertia of the second mode vanishes with the result that the second natural frequencies of both systems goes to infinity and with it the entire second passband. The first natural frequencies of the free and the fixed blade systems approach the distinct values given in Table A1. If, conversely, the disk mass is infinitely higher than the blade mass, $\bar{m} \to \infty$, the system is equivalent to a cantilevered blade and the coupling spring has no effect. The first mode of both systems, in which the masses move in phase, becomes a rigid body mode with $\bar{\omega} = 0$. The second natural frequency of both systems approaches the blade natural frequency, $\bar{\omega} = 1$. Thus, both passbands narrow to a single frequency.

Figure A2 shows a parametric study of the natural frequencies of a 50-blade assembly. Since the number of blades is even, the passbands are bounded by the lowest and the highest natural frequencies. The most important feature of the system is illustrated in Fig. A2(c). For high values of $\bar{k}_c$, the natural frequencies in the first passband are densely spaced at the right (upper) passband edge — all except the first one. This is not surprising since the first mode has all bays vibrating in phase, unaffected by the coupling spring, whereas all other modes require some stretching of the very stiff spring. Thus, it is as if the blades are mounted on the perimeter of a rigid ring and all frequencies but one approach the natural frequency of a cantilevered blade. The first frequency corresponds to a mode in which there is rigid rotation of the ring. Note also the implications of this behavior with respect to the midband frequency ($\sigma = \pi/2$): The midband frequency merges with the right passband edge and is no longer located close to the average frequency of the passband. The modal density at the midband frequency tends to infinity.

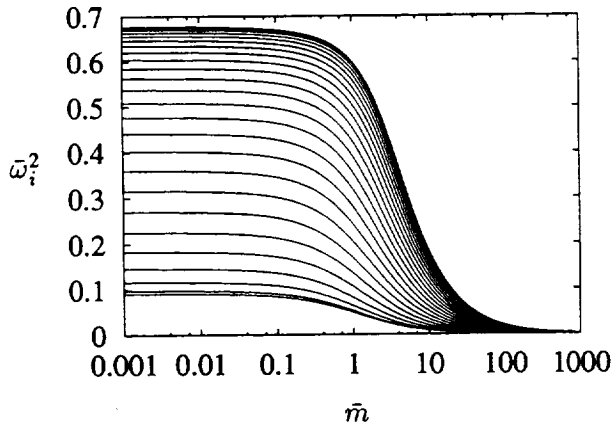

(a) $\bar{k}_c = 1$, $\bar{k}_d = 1$, ***1st passband***

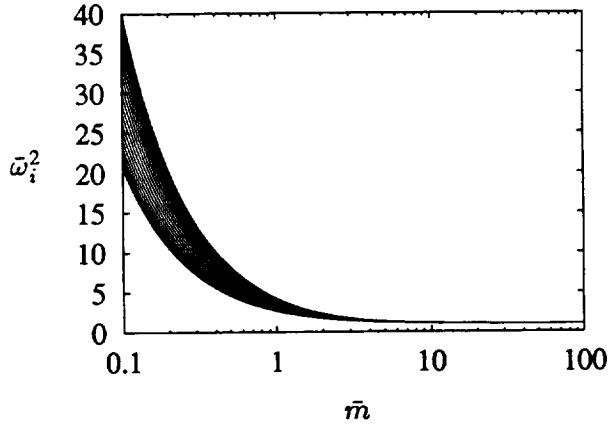

(b) $\bar{k}_c = 1$, $\bar{k}_d = 1$, ***2nd passband***

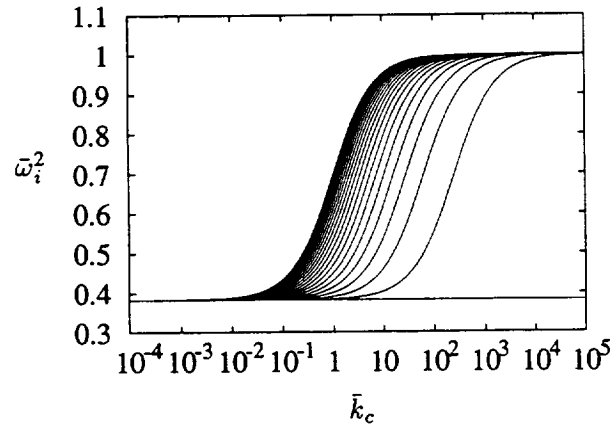

(c) $\bar{m} = 1$, $\bar{k}_d = 1$, ***1st passband***

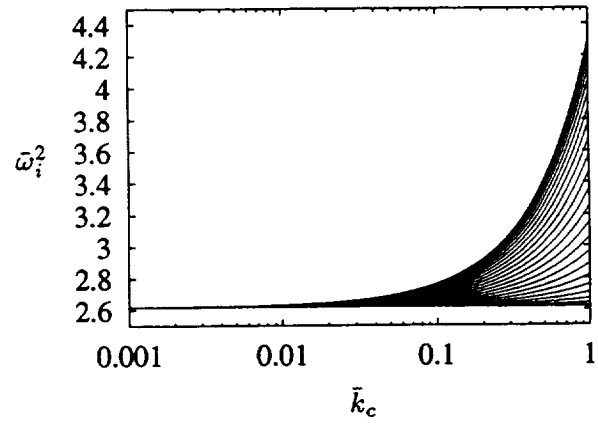

(d) $\bar{m} = 1$, $\bar{k}_d = 1$, ***2nd passband***

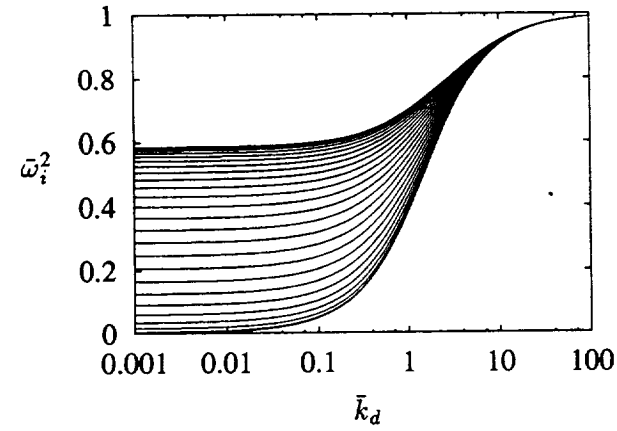

(e) $\bar{k}_d = 1$, $\bar{m} = 1$, ***1st passband***

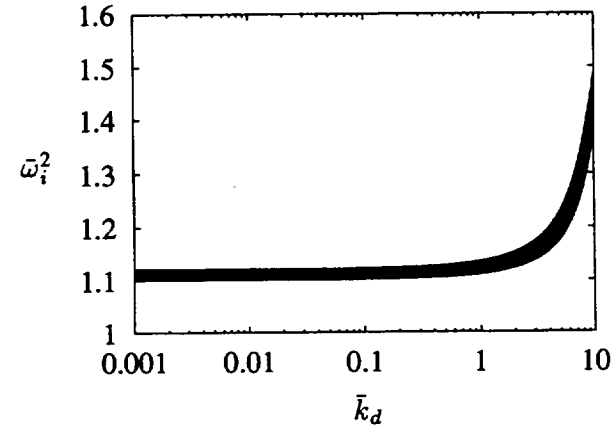

(f) $\bar{k}_d = 1$, $\bar{m} = 10$, ***2nd passband***

Figure A2 Natural frequencies of a 50-blade assembly, plotted as a function one of $\bar{k}_d$, $\bar{k}_c$ and $\bar{m}$ with the other two fixed. Since the number of blades is even, the lowest and the highest frequencies are also the bounding frequencies of the passband.

REPORT DOCUMENTATION PAGE

Form Approved
OMB No. 0704-0188

1. AGENCY USE ONLY (*Leave blank*)	2. REPORT DATE	3. REPORT TYPE AND DATES COVERED
	May 1993	Technical Memorandum

4. TITLE AND SUBTITLE

A Transfer Matrix Approach to Vibration Localization in Mistuned Blade Assemblies

5. FUNDING NUMBERS

WU-505-62-21

6. AUTHOR(S)

Gisli Ottarsson and Christophe Pierre

7. PERFORMING ORGANIZATION NAME(S) AND ADDRESS(ES)

National Aeronautics and Space Administration
Lewis Research Center
Cleveland, Ohio 44135-3191

8. PERFORMING ORGANIZATION REPORT NUMBER

E-7764

9. SPONSORING/MONITORING AGENCY NAME(S) AND ADDRESS(ES)

National Aeronautics and Space Administration
Washington, D.C. 20546-0001

10. SPONSORING/MONITORING AGENCY REPORT NUMBER

NASA TM-106112
ICOMP-93-10

11. SUPPLEMENTARY NOTES

Gisli Ottarsson, The University of Michigan, Ann Arbor, Michigan 48109-2125 and Christophe Pierre, Institute for Computational Mechanics in Propulsion, Lewis Research Center, Cleveland, Ohio and The University of Michigan, Ann Arbor, Michigan 48109-2125 (work funded under NASA Cooperative Agreement NCC3-233). ICOMP Program Director, Louis A. Povinelli, (216) 433-5818.

12a. DISTRIBUTION/AVAILABILITY STATEMENT

Unclassified - Unlimited
Subject Category 39

12b. DISTRIBUTION CODE

13. ABSTRACT ***(Maximum 200 words)***

A study of *mode localization* in *mistuned bladed disks* is performed using *transfer matrices*. The transfer matrix approach yields the free response of a *general*, mono-coupled, perfectly cyclic assembly in closed form. A *mistuned* structure is represented by *random* transfer matrices, and the expansion of these matrices in terms of the small mistuning parameter leads to the definition of a measure of *sensitivity* to mistuning. An approximation of the *localization factor*, the spatially averaged rate of exponential attenuation per blade-disk sector, is obtained through *perturbation techniques* in the limits of high and low sensitivity. The methodology is applied to a common model of a bladed disk and the results verified by *Monte Carlo simulations*. The easily calculated sensitivity measure may prove to be a valuable design tool due to its system-independent quantification of mistuning effects such as mode localization.

14. SUBJECT TERMS	15. NUMBER OF PAGES
Aeroelasticity; Mistuned bladed-disks; Mode localization; Sensitivity measure; Transfer matrices	40
	16. PRICE CODE A03

17. SECURITY CLASSIFICATION OF REPORT	18. SECURITY CLASSIFICATION OF THIS PAGE	19. SECURITY CLASSIFICATION OF ABSTRACT	20. LIMITATION OF ABSTRACT
Unclassified	Unclassified	Unclassified	

National Aeronautics and
Space Administration

Lewis Research Center
ICOMP (M.S. 5-3)
Cleveland, Ohio 44135

FOURTH CLASS MAIL

ADDRESS CORRECTION REQUESTED

NASA